Polyphenols promote stem cell surface adaptation onto low-adhesion chitosan-titanium through protein synthesis and cytoskeletal remodeling

Biomaterials Advances 180 (2026) 214584

Contents lists available at ScienceDirect

Biomaterials Advances

journal homepage: www.journals.elsevier.com/materials-science-and-engineering-c

Polyphenols promote stem cell surface adaptation onto low-adhesion chitosan-titanium through protein synthesis and cytoskeletal remodeling

Farah Daou [a], Camilla Reggio [b], Marcello Manfredi [c], Hugo Abreu [a], Giuseppe Cappellano [a], Mauro Nascimben [a], Gissur Örlygsson [d,e], Chuen H. Ng [e], Antonella Bosso [f], Sara Ferraris [b], Silvia Spriano [b,*], Andrea Cochis [a]

[a] Department of Health Sciences, Center for Translational Research on Autoimmune and Allergic Diseases CAAD, Università del Piemonte Orientale UPO, Italy
[b] Politecnico di Torino, Corso Duca degli Abruzzi 24, 10129, Turin, Italy
[c] Department of Translational Medicine, Center for Translational Research on Autoimmune and Allergic Diseases CAAD, Università del Piemonte Orientale UPO, Italy
[d] IceTec, Arleynir 8, 112, Reykjavik, Iceland
[e] Genis, Adalgata 34, 580, Siglufjördur, Iceland
[f] Consiglio per la ricerca in agricoltura e l'analisi dell'economia agraria—Centro di Ricerca Viticoltura ed Enologia, via P. Micca 35, 14100, Asti, Italy.

ARTICLE INFO

Keywords:
Proteomics
Polyphenols
Adhesion
Titanium
Chitosan
Bone implants

ABSTRACT

Implant surface modification aims to facilitate integration by enhancing cell-material interactions at the interface. Accordingly, a Ti6Al4V alloy was chemically treated to obtain a microtextured topography with a high density of reactive -OH groups, then coated with chitosan and finally functionalized with a polyphenol extract from white grape seeds. Chitosan was crosslinked with sodium tripolyphosphate to reduce swelling. The extract and the functionalization solution were analyzed through HPLC, DLS, zeta potential, Folin-Ciocalteu assay, and UV–Vis spectroscopy. The functionalized Ti alloys were characterized through fluorescence and XPS analysis. The biological characterization using human bone marrow-derived stem cells (hBM-MSCs) showed low adhesion on chitosan, while polyphenols significantly improved surface colonization. Immunocompatibility studies using peripheral blood mononuclear cells excluded alterations in the balance of immune cell subsets due to the interaction with the polyphenol-functionalized titanium. Proteomic studies were performed on proteins expressed by hBM-MSCs and on proteins adsorbed from a rich protein source such as fetal bovine serum (FBS). Results demonstrated that polyphenols enhanced protein synthesis and extracellular matrix organization for hBM-MSCs, while they significantly promoted the adsorption of proteins from FBS.

1. Introduction

In Orthopedics and Dentistry implantology, one of the prevalent challenges is the failure of implants [1,2]. This failure is predominantly attributed to inadequate sealing at the interface between the implant and the bone, a key factor for restoring damaged or lost bone tissue and the long-term stability of implants [3]. The following objectives must be met for successful bone regeneration. Firstly, an optimal integration between the implant and the surrounding bone tissue is needed for adequate mechanical stability and to prevent early microcracks [4]. Secondly, sufficient bone healing and regeneration at the implant site is critical in large bone defects or compromised bone quality [5]. Lastly, preventing infection and chronic inflammation is crucial for effective bone regeneration [6]. So, multifunctional materials must be designed to facilitate the achievement of these endpoints [7].

Surface modification of bioinert titanium alloys is widely investigated to get osteoconductivity, osteoinduction ability, high scratch and fatigue resistance, and long-term stability of bone implants. Surface modifications and coatings can be classified into physical-mechanical, chemical, and biological. Physical-mechanical methods alter the topography of the Ti interface, such as sandblasting and e-beam or laser surface engineering, and increase the focal adhesion of osteoblasts and bone-implant contact through micro- and nano-roughness [8]. Chemical methods modify the topography and increase the thickness of the surface oxide layer for faster osteointegration and higher corrosion resistance of titanium, such as acid etching, anodic oxidation, and micro-arc oxidation [65]. Biological methods involve antimicrobial and pro-regenerative bioactive coatings [9]. Chitosan (CH) is an FDA-approved

* Corresponding author.
E-mail address: silvia.spriano@polito.it (S. Spriano).

https://doi.org/10.1016/j.bioadv.2025.214584
Received 14 July 2025; Received in revised form 13 October 2025; Accepted 29 October 2025
Available online 4 November 2025

polymer with biocompatibility, anti-inflammatory, and antibacterial properties of interest for coating of biomaterials for wound dressing [10]. As an example, Villegas et al. [11] demonstrated that CH-coated medical-grade titanium alloy facilitated cell adhesion while preventing biofilm formation, but there is no general agreement on these effects.

Polyphenols enhance cellular adhesion and have strong anti-inflammatory properties [12], but they are not significantly bioavailable when delivered through food and metabolized through the intestinal tract. The idea is to use them in the surface functionalization of biomaterials to be locally bioavailable and more chemically stable, largely exercising their properties [13,14]. On the other hand, a synergic action of polyphenols and CH can be expected [15,16].

Based on the current state of the art [17,18], previous studies have largely concentrated on evaluating the physico-chemical and general biological properties of these synergistic coatings. As such, there is a critical gap in our understanding of the specific molecular mechanisms related to how these coatings regulate the cell-material interface. Based on these premises, and to the best of our knowledge, our work advances the field by being the first to apply a comprehensive proteomic analysis and novel bioinformatic methods (e.g., outlier detection) to precisely map the cellular protein expression changes. Accordingly, surfaces were chemically treated by a protocol patented by the Authors [19] to obtain a random micro- and nano-porosity (named Ti-CT) and a high surface density of OH groups with acidic reactivity. This step aims to make the titanium surface suitable to be coated. Then, a layer of CH was deposited onto the Ti-CT surfaces and tripolyphosphate polyanion (TPP) was used as a crosslinker to enhance mechanical properties and chemical resistance and to control permeability, solubility and degradation of CH [16]. Finally, polyphenols were extracted from seeds in the unfermented grape pomace of Moscato Bianco grapes and used to functionalize the CH layer. Extracts from seeds of unfermented Moscato grapes were selected because they are extremely rich in active polyphenols (high GAE and DPPH values as an index of polyphenols content and antiradical activity) and have a potential for medical/pharmacological applications [20]. Moreover, the extract used in this research comes from the by-product of the wine industry, with responsible use and valorization of local resources in line with a circular economy approach. In fact, grape pomaces represent an abundant (more than 1 Mt./year in the world) and environmentally impactful byproduct difficult to be properly disposed (low pH, and poor biodegradation) [21,22]. The valorization of grape pomaces can have strong economic, environmental, and social impacts. The extract, functionalization solution and resulting titanium specimens underwent a series of physicochemical characterizations by means of HPLC, DLS, zeta potential, Folin& Ciocalteau test, UV–Vis spectroscopy, fluorescence microscopy, and XPS analysis. To evaluate the coating's biocompatibility, we assessed its cytocompatibility with human bone marrow-derived stem cells (hBM-MSCs) and immunocompatibility with peripheral blood mononuclear cells (PBMCs). We also analyzed the cellular, using hBM-MSCs, and molecular, using fetal bovine serum (FBS), proteomic profiles. To better interpret these proteomic results, we employed bioinformatic outlier detection to identify significant protein expression changes. Lastly, considering the variable antibacterial effects reported for chitosan and polyphenols, we performed a preliminary evaluation of the coating against *Staphylococcus aureus*.

2. Materials and methods

2.1. Sample preparation

2.1.1. Ti-CT

Ti6Al4V discs (ASTM B348 -Titanium Consulting, Bagno a Ripoli, Firenze, Italy – discs 10 mm in diameter and 2 mm thick) were polished using SiC papers (P320-4000). The samples were washed in an ultrasonic bath once in acetone (Sigma-Aldrich, Inc., St. Louis, MO, United States) for 5 min and twice in ultra-pure water for 10 min each. The chemical treatment was performed after drying the samples under a fume hood at room temperature. The treatment was described in [19]. It consists of etching the alloy in HF (Sigma-Aldrich, Inc., St. Louis, MO, United States) to remove the native oxide, followed by controlled oxidation in hydrogen peroxide (Panareac). After the chemical treatment, the titanium samples were activated to enhance surface reactivity and remove any contaminants by exposure to UV irradiation for 1 h (UV-C 40 W; 253.7 nm). The chemically treated samples were named Ti-CT.

2.1.2. Ti-CT-CH and Ti-CT-CH-TPP

CH used for coating Ti-CT samples is G060724P (Genis, Iceland) with a deacetylation degree of 50 %. The powders were dissolved in 1 % acetic acid (Sigma-Aldrich, Inc., St. Louis, MO, United States) at room temperature to a concentration of 0.75 *w/v*%. The Ti-CT samples were coated with 78 µl of the CH solution pipetted onto the surface and left to dry under a fume hood at room temperature. The chemically treated and CH-coated titanium samples were named Ti-CT-CH.

For CH crosslinking, the titanium-coated specimens (Ti-CT-CH) were immersed in a 15 % w/v TPP solution (Sigma Aldrich). The pH of the solution was adjusted to 6 with a phosphoric acid solution (Sigma-Aldrich, Inc., St. Louis, MO, United States). The titanium samples chemically treated, CH-coated, and crosslinked were named Ti-CT-CH-TPP.

2.1.3. Ti-CT-CH-TPP-PPHE

The polyphenols used for functionalization were extracted from seeds in the unfermented grape pomace of Moscato Bianco grapes. The solution for functionalization was prepared by solubilizing the extract (PPHE) at a concentration of 5 mg/ml in a TRIS+HCl buffer (Sigma-Aldrich, Inc., St. Louis, MO, United States) and adding $CaCl_2$ (0.292 g/l). The solution was stirred with a magnetic stirrer for 1 h at room temperature and filtered through a 0.2 µm filter. The functionalization solution was named PPHE-TRIS-Ca. The Ti-CT-CH-TPP samples were functionalized in 2 ml of PPHE-TRIS-Ca by incubation for 3 h at 37 °C, rinsed with ultra-pure water, and dried under a fume hood at room temperature. The titanium samples chemically treated, coated (crosslinked), and functionalized were named Ti-CT-CH-TPP-PPHE.

All samples for cell tests were prepared under clean conditions by sterilizing in an autoclave water, glassware and tweezers, packaged and subsequently sterilized with γ radiation at 25 kGy.

2.2. Physical-chemical characterization

The chemical composition of the extract was analyzed by HPLC. The operating protocol is described in [23,24]. The total condensed tannin content, their mean degree of polymerization (mDP), and the percentage of each constitutive unit were determined by the phloroglucinolysis reaction and the HPLC analysis of the reaction products. Monomer flavan-3-ols ((+)-catechin and (–)-epicatechin) were determined with the same HPLC method used for the phloroglucinolysis method, excluding the reaction with phloroglucinol.

The functionalization solution (PPHE-TRIS-Ca) was analyzed by measuring the zeta potential and hydrodynamic radius with an electrophoretic analyzer (DLS - Litesizer 500, Anton Paar, Gratz, Austria). As a comparison, a solution of the extract (5 mg/ml) in water, buffered at pH 7.4 with HCl and NaOH and filtered (0.2 µm) was also measured (named PPHE-W-7.4). This analysis was performed in triplicate.

The Folin–Ciocalteu test (F&C) was used to measure the redox reactivity of phenolic substances and quantify their amount (as Gallic Acid Equivalents, GAE) in a solution using a calibration curve with gallic acid as the standard, measuring the absorbance at 760 nm. The colour of the solution results from the redox reaction between the Folin–Ciocâlteu reagent (Folin–Ciocâlteu phenol reagent, Sigma-Aldrich, Inc., St. Louis, MO, United States), which contains phosphotungstic/phosphomolybdic acids and polyphenols. The measurement was performed through UV–Vis spectroscopy (Spectrophotometer UV-2600, Shimadzu). The test was performed on PPHE-TRIS-Ca and PPHE-W, a filtered (0.2 µm)

solution of the extract (5 mg/ml) in water. This analysis was performed in triplicate. The same UV–Vis spectrometer was used to measure the absorbance spectra (200–800 nm) of PPHE-TRIS-Ca and PPHE-W solutions.

Ti-CT-CH-TPP and Ti-CT-CH-TPP-PPHE were observed through fluorescence microscopy (LSM 900, Zeiss, Dusseldorf, Germany) and the images were processed by using Zen software (Axio Imager 2, Zeiss), exploiting polyphenols' autofluorescence. A red filter and excitation wavelength of 573 nm were used.

The chemical composition of Ti-CT-CH-TPP and Ti-CT-CH-TPP-PPHE was analyzed by X-ray photoelectron spectroscopy (XPS, PHI 5000 VERSA PROBE, PHYSICAL ELECTRONICS). Both survey and high-resolution spectra of carbon and oxygen regions were acquired. All the high-resolution spectra were referenced by setting the hydrocarbon C1s peak to 284.80 eV for charging effect compensation.

2.3. In vitro cytocompatibility studies

For in vitro cytocompatibility studies, the International Organization for Standardization (ISO) 10993-5:2009 (Biological evaluation of medical devices — Part 5: Tests for in vitro cytotoxicity) standard [66] was followed.

2.3.1. Cell culture conditions

Human telomerase reverse transcriptase (hTERT) immortalized hBM-MSCs of clonal line Y201, which was generated and kindly provided by James et al. [25], were cultivated in Dulbecco's modified Eagle medium-low glucose (DMEM-LG, Gibco) supplemented with 15 % fetal bovine serum (FBS, Merck) and 1 % antibiotics (Penicillin-Streptomycin, Merck). The cells were maintained at 37 °C in a 5 % CO_2 atmosphere. Upon reaching 80–90 % confluence, the cells were collected by enzymatic digestion using trypsin/ethylenediamine tetraacetic acid (Trypsin-EDTA, Merck) before each assay.

2.3.2. Cell seeding

hBM-MSCs were seeded directly onto the surface of the titanium discs placed in a 24-well cell culture plate. The cells were seeded at a specific density of 2×10^4 cells/specimen in a defined volume of 100 µl. After allowing the cells to adhere for 4 h, 1 ml of fresh cell culture medium was added to cover the samples, which were then incubated for 24 h in direct contact with cells.

2.3.3. Resazurin reduction assay

The resazurin reduction assay was used to evaluate cells' metabolic activity, which can be correlated with the viability of metabolically active cells. The mother solution was prepared by dissolving resazurin sodium salt (powder, Merck) in 1× phosphate-buffered saline (PBS) to get a 1 % resazurin solution. After 24 h of incubation of the titanium discs with hBM-MSC, the spent cell culture medium was discarded, and the samples were rinsed with PBS and transferred to a new 24-well cell culture plate. Each well was then supplemented with 1 ml of the resazurin working solution (0.015 % [*v*/v] in cell culture medium). Following 3 h of incubation, fluorescence measurements were taken using a Tecan GENios Microplate Reader (Spark, Tecan Trading AG) with excitation and emission wavelengths set at 530 and 590 nm, respectively. The obtained results were based on three biological replicates per group ($n = 3$).

2.3.4. Cell adhesion and morphology

For the examination of cell adhesion and morphology, a scanning electron microscope (SEM) (JSM-IT500, JEOL, Italy) was used. After 24 h of incubation, the spent cell culture medium was discarded, the titanium discs were gently washed with PBS, and the attached cells were fixed using 2.5 % glutaraldehyde. The samples were stored overnight at 4 °C. Afterwards, glutaraldehyde was dispensed and the samples were washed with PBS and dehydrated in a graded alcohol solution (70 %, 90 %, and 100 % twice). The samples were then covered with hexamethyldisilazane (HMDS) for 30 min and air-dried in a chemical fume hood. Finally, to enhance conductivity, the samples were coated with gold using a sputter coating machine (DII-29030SCTR Smart Coater, JEOL, Italy).

2.3.5. Lactate dehydrogenase (LDH) release assay

Cell membrane damage was quantified after 24 h of culturing by measuring lactate dehydrogenase (LDH) release using the CyQUANT™ LDH Cytotoxicity Assay Kit (Thermo Fisher Scientific), following the manufacturer's protocol. To establish the maximum LDH release control, three wells were treated with 10 µl of lysis buffer and incubated for 45 min at 37 °C. Subsequently, 50 µl of conditioned medium was collected from each of the following: (1) the experimental wells with cells seeded on the top of the titanium discs (Sample LDH Activity); (2) untreated control wells with cells directly onto the wells of a 24-well plate (Spontaneous LDH Activity); and (3) the lysed cell wells (Maximum LDH Activity). The conditioned media from all three groups were transferred to a 96-well plate, and the LDH reaction mixture was added. After 10 min of incubation, the stop solution was added to the well, and fluorescence was measured using Tecan GENios Microplate Reader (Spark, Tecan Trading AG) with an excitation of 560 nm and an emission of 590 nm. After subtracting the background fluorescence from all readings, the percentage of cytotoxicity was calculated using the formula: % Cytotoxicity = [(Sample LDH Activity - Spontaneous LDH Activity) / (Maximum LDH Activity - Spontaneous LDH Activity)] x 100.

2.4. In Vitro immunocompatibility studies

2.4.1. Blood sample collection

Peripheral blood samples (10 ml each) were collected from six healthy adult donors (25–45 years old) in collaboration with the Hospital Maggiore della Carità, Novara, Italy, into lithium heparin tubes and processed immediately. The study was ethically approved (prot. n. 675/CE) by the local committee.

2.4.2. Peripheral blood mononuclear cells (PBMCs) isolation

The collected peripheral blood samples were mixed with PBS in a 1:1 ratio. In a separate tube, 15 ml of lympholyte solution (Cedarlane, Canada) was combined with 20 ml of the diluted blood. The resulting mixture underwent centrifugation at 1800 rpm for 20 min, with an acceleration rate of 1 and a deceleration rate of 0. After centrifugation, the ring of peripheral blood mononuclear cells (PBMCs) was collected. These PBMCs were then combined with 10 ml of RPMI 1640 Medium (Gibco, USA) supplemented with 10 % FBS. The resulting solution underwent further centrifugation at 1500 rpm for 5 min, yielding a cell pellet which was resuspended in 5 ml of complete cell culture medium. Subsequently, 1×10^6 PBMCs in 1 ml of cell culture medium were added to titanium discs placed in a 24-well cell culture plate. The Ti-CT-CH discs were excluded due to the limited number of PBMCs that can be collected from each donor and due to the weak cell attachment, as evidenced by the in vitro cytocompatibility studies.

2.4.3. Fluorescence-activated cell sorting (FACS) analysis

After 72 h of incubation, cells were harvested from titanium discs in FACS tubes and centrifuged at 1500 rpm for 5 min, as previously described (Abreu et al. [26]; Abreu et al. [27]). Then, cells were washed with PBS-EDTA 2 mM and stained with a viability dye (BD Horizon™ Fixable Viability Stain 780) for 15 min, at 4 °C. After wash, Human BD™ Fc block solution was added. Antigen surface staining was performed by adding an antibody mix containing the following monoclonal antibodies (mAb): mouse antiCD3 BUV496 (clone: UCHT1), antiCD4 BUV737 mAb (clone: SK3), antiCD8 BUV805 mAb (clone: SK1), antiCD25 APC-R700 mAb (clone: 2A3), antiCD45 BUV395 mAb (clone: HI30), antiCD127 BV786 mAb (clone: HIL-7R-M21), antiCD45RA BUV563 mAb (clone: HI100), antiCD183 APC mAb (clone: IC6), antiCD194 PE-CF594 mAb

(clone: 1G1), antiCD196 BV480 mAb (clone: 11A9) and antiCD197 BV711 mAb (clone: 150503) in BD Horizon™ Brilliant Stain Buffer for 20 min, at 4 °C. Lastly, the cells were washed and resuspended in PBS-EDTA for acquisition using a BD FACSymphony™ A5 flow cytometer. Data were then analyzed using the BD FACSDIVA™ software version 9.0. All reagents were purchased from Becton and Dickinson (Franklin Lakes, NJ, USA). Fluorescence minus one (FMO) was used as a control.

2.5. Cellular proteomic studies

2.5.1. Cell collection

For proteomic analysis, Ti-CT and Ti-CT-CH-TPP-PPHE were seeded with hBM-MSC as detailed in Section 2.3.2 in triplicate ($n = 3$) and incubated for 24 h. The adhered cells were detached by adding 1 ml of collagenase type I (3 mg/ml, Merck) in trypsin/EDTA (Merck) per sample and incubating for 10–15 min at 37 °C. After deactivating the enzymes with 2 ml of cell culture medium, the samples were washed with PBS to ensure the collection of all cells. Finally, the detached cells were collected for further analysis.

2.5.2. Protein extraction and trypsin digestion

The cells were lysed using 200 µl of radioimmunoprecipitation assay buffer (RIPA buffer) containing 50 mM TrisHCl (pH 7.2), 0.5 mM EDTA, 0.1 % NP40, and 0.05 % SDS. To ensure complete lysis, the lysate underwent 5 cycles of sonication. The protein concentration in the lysate was determined using the Bradford protein assay, with bovine serum albumin (BSA) as the standard.

2.5.3. Sample preparation

Following the initial steps, the samples underwent reduction using 200 mM dithiothreitol (DTT) and alkylation with 200 mM iodoacetamide (IAM). Protein digestion was then carried out using trypsin (Sigma-Aldrich Inc., St. Louis, MO, United States). The resulting tryptic peptides were desalted using a Discovery® DSC-18 solid phase extraction (SPE) 96-well plate (25 mg/well) from Sigma-Aldrich Inc., St. Louis, MO, United States. Before loading the sample, the SPE plate was preconditioned with 1 ml of acetonitrile and 2 ml of water. The sample was then loaded and washed with 1 ml of water. The adsorbed proteins were eluted with 800 µl of acetonitrile: water (80,20). After the desalting process, the sample was vacuum-evaporated and reconstituted in the mobile phase for subsequent analysis.

2.5.4. Proteomics analysis and data processing

The digested peptides were analyzed with an EASY nano-LC1200 system (Thermo Scientific, Milano, Italy) coupled to a 5600+ TripleTOF system (AB Sciex, Concord, Canada). The following liquid chromatography parameters were used: analytical column Acclaim PepMap C18 2 µm 75 µm × 150 mm and injection volume 2 µl. The flow rate was 300 nl/min, phase A was 0.1 % formic acid/water, and phase B was 80 % acetonitrile/0.1 % formic acid/20 % water. A 2-hour gradient was used (3–45 %). For identification purposes the mass spectrometer analysis was performed using a mass range of 100–1600 Da (TOF scan with an accumulation time of 0.25 s), followed by an MS/MS product ion scan from 400 to 1250 Da (accumulation time of 5.0 ms) with the abundance threshold set at 30 cps (40 candidate ions can be monitored during every cycle). The ion source parameters in electrospray positive mode were set as follows: curtain gas (N2) at 30 psig, nebulizer gas GAS1 at 25 psig, ion spray floating voltage (ISFV) at 2700 V, source temperature at 90 °C and declustering potential at 85 V. For label-free quantification, samples were then subjected to cyclic data independent analysis (DIA) of the mass spectra, using a 25-Da window. A 50 ms survey scan (TOF-MS) was performed, followed by MS/MS experiments on all precursors. These MS/MS experiments were performed in a cyclic manner using an accumulation time of 40 ms per 25-Da swath (36 swaths in total) for a total cycle time of 1.5408 s. The ions were fragmented for each MS/MS experiment in the collision cell using the rolling collision energy. The MS data were acquired with Analyst TF 1.7 (SCIEX, Concord, Canada). The mass spectrometry files were searched using Protein Pilot (AB SCIEX, Concord, Canada) and Mascot (Matrix Science Inc., Boston, United States). Samples were input into Protein Pilot software v. 4.2 (AB SCIEX, Concord, Canada), with the following parameters: cysteine alkylation, digestion by trypsin, no special factors, and False Discovery Rate set at 1 %. The UniProt Swiss-Prot reviewed database containing human proteins was used (version 01/02/2018, containing 42,271 sequence entries) and the Mascot search was performed on Mascot v. 2.4, where the digestion enzyme selected was trypsin, with 2 missed cleavages and a search tolerance of 50 ppm was specified for the peptide mass tolerance, and 0.1 Da for the MS/MS tolerance. The charges of the peptides to search for were set at 2 +, 3 +, and 4 +, and the search was set on monoisotopic mass. The instrument was set at ESI-QUAD-TOF and the following modifications were specified for the search: carbamidomethyl cysteines as a fixed modification, and oxidized methionine as a variable modification. The quantification was performed by integrating the extracted ion chromatogram of all the unique ions for a given peptide. The quantification was carried out with PeakView 2.2 and MarkerView 1.2 (Sciex, Concord, ON, Canada). Six peptides per protein and six transitions per peptide were extracted from the SWATH files. Shared peptides were excluded, as well as peptides with modifications. Peptides with FDR lower than 1.0 % were exported in MarkerView for the *t*-test.

Statistical analyses on protein abundances were performed using MetaboAnalyst software [67] (https://www.metaboanalyst.ca/). Differentially expressed proteins were filtered using the following thresholds: p-value <0.5 and fold-change ≥ 1.5. The differentially upregulated and downregulated proteins were analyzed separately using the STRING database [28] and Database for Annotation, Visualization and Integrated Discovery (DAVID) (version 6.8) (http://david.abcc.ncifcrf.gov/).

2.6. Molecular proteomic studies

2.6.1. Protein adsorption using fetal bovine serum (FBS)

To prepare the titanium discs for the analysis, the discs were immersed in 100 % commercial fetal bovine serum (FBS, Merck) and allowed to incubate for 2 h at 37 °C in a 5 % CO_2 atmosphere in triplicate ($n = 3$). After the incubation period, the samples were rapidly washed with PBS to remove any excess FBS. Using a cell scraper, each titanium disc was gently scraped to collect the adhered proteins, and the collected proteins were suspended in a total volume of 500 µl of ultrapure water.

2.6.2. Protein quantification

Protein concentration was measured with Bradford protein assay (Sigma-Aldrich, St. Louis, MO) using BSA as a standard.

2.6.3. Proteomics analysis and data processing

Specimens were prepared as detailed in 2.5.3. The digested peptides were analyzed with a UHPLC Vanquish system (Thermo Scientific, Rodano, Italy) coupled with an Orbitrap Q-Exactive Plus (Thermo Scientific, Rodano, Italy). Peptides were separated by a reverse phase column (Accucore™ RP-MS 100 × 2.1 mm, particle size 2.6 µm). The column was maintained at a constant temperature of 40 °C at a flow rate of 0.2 ml/min. Mobile phases A and B were water and acetonitrile, respectively, both acidified with 0.1 % formic acid. The analysis was performed using the following gradient: 0–5 min from 2 % to 5 % B; 5–55 min from 5 % to 30 % B; 55–61 from 30 % to 90 % B and hold for 1 min, at 62.1 min the percentage of B was set to the initial condition of the run at 2 % and hold for about 8 min to re-equilibrate the column, for a total run time of 70 min. The mass spectrometry analysis was performed in positive ion mode. The electrospray ionization (ESI) source was used with a voltage of 2.8 kV. The capillary temperature, sheath gas flow, auxiliary gas, and spare gas flow were set at 325 °C, 45 arb, 10 arb, and 2 arb, respectively. S-lens was set at 70 rf. For the acquisition of spectra, a data-dependent (ddMS2) top 10 scan mode was used. Survey

full-scan MS spectra (mass range m/z 381 to 1581) were acquired with resolution $R = 70{,}000$ and AGC target 3×106. MS/MS fragmentation was performed using high-energy c-trap dissociation (HCD) with resolution $R = 35{,}000$ and automatic gain control (AGC) target 1×106. The normalized collision energy (NCE) was set to 30. The injection volume was 6 μl. The mass spectra analysis was conducted using MaxQuant software (version 1.6.14). The software was configured with specific parameters for the analysis. Trypsin was selected as the enzyme specificity for peptide digestion. The search parameters included an initial precursor ion tolerance of 10 ppm and an MS/MS tolerance of 20 ppm. Carbamidomethylation was set as a fixed modification, while oxidation was considered a variable modification. The maximum number of allowed missed cleavages was set to 2. The analysis utilized Uniprot *Bos Taurus* sequence database. For label-free quantification, the analysis included a "match between runs" option. The protein and peptide false discovery rate (FDR) was set to 0.01. Quantification was based on extracted ion chromatograms, with a minimum ratio count of 1. Additionally, a minimum required peptide length of 7 amino acids was set for accurate quantification.

Statistical analysis was performed as detailed in 2.5.4.

2.7. Statistical analysis of data

All experiments were run with three biological replicates, except for the immunocompatibility study ($n = 6$), and the data were represented as means ± standard deviation (SD). Before the analysis, the normality of continuous variables was assessed. Comparisons between groups were conducted using ANOVA, and statistical significance was defined as p-value <0.05. The analysis was conducted using R (R Core Team, 2020), RStudio (Rstudio Team, 2020), and the tidyverse package (Wickham, 2017).

2.8. Outliers detection

Proteomics outlier detection was included in the current analysis to identify data points (e.g., proteins, peptides, or spectral counts) that significantly deviate from expected values due to biological reasons. The approach included dimensionality reduction using the UMAP [29] algorithm and machine learning techniques such as Isolation Forest. The biological replicates were transformed into 2D embeddings through UMAP to simplify anomaly expression recognition, followed by Isolation Forest [30], which provided a tree-based method to isolate and detect anomalies. Preliminary preprocessing of the mass spectrometer peak area involved normalization and log transformation. The mass spectrometer peak area refers to the area under a specific peak in a mass spectrum, representing the amount or concentration of a particular ion detected by the instrument. The area is proportional to the abundance or intensity of the ion, indicating how much of that ion is present in the sample and, consequently, is proportional to the protein's concentration; a larger peak area typically shows a higher abundance of the corresponding protein.

Functional profiling of the outlier genes was carried out with G:Profiler [31] Python library, and reporting outcomes with the following abbreviations (Tables 4M and 6M): "GO:BP" is for Gene Ontology Biological Process, "GO:CC" is for Gene Ontology Cellular Component, and "GO:MF" is for Gene Ontology Molecular Function. Molecular pathways were collected from "KEGG", "Reactome" (REACT in the tables), and "WikiPathways" (WP in the tables). Regulatory motif matches are from "TRANSFAC" (abbreviated as TF), and protein complexes data are from "CORUM." Additionally, miRNA targets are from "miRTarBase" (abbr. MIRNA).

3. Results

3.1. Physical-chemical characterization

The chemical composition of the PPHE extract, analyzed by HPLC, is reported in Table 1. The total polyphenol content (GAE index) is directly related to the antiradical capacity (DPPH) of the extracts [20].

The flavonoid fraction was constituted by flavanols, condensed tannins (oligomers: dimers B1, B2 and B3 and trimer C1 and polymers) and monomeric flavan-3-ols ((+)-catechin, (−)-epicatechin and (−)-epicatechin-3-O-gallate), while it did not include anthocyanins and flavonols (e.g. quercetin, myricetin).

The functionalization solution (PPHE-TRIS-Ca) was prepared by solubilizing the extract in a buffer (TRIS+HCl; pH 7.4), added with Ca^{2+} ions. PPHE-TRIS-Ca showed a hydrodynamic radius of approximately 62 nm with a polydispersity index of approximately 25 nm (DLS characterization).

The zeta potential of PPHE-TRIS-Ca was measured at −12 mV, while it was −22 mV in the case of PPHE-W-7.4 (a solution at pH 7.4 of the extract without the addition of Ca^{2+}).

The Folin-Ciocalteu test measured a GAE (gallic acid equivalents) value of 1.9 ± 0.1 mg/ml on PPHE-TRIS-Ca. The GAE value of PPHE-W (without calcium ions) was 1.5 ± 0.1 mg/ml.

The UV–Vis spectra of PPHE-TRIS-Ca and PPHE-W (Fig. 1) showed an absorption peak at 280 nm typical of polyphenols. PPHE-TRIS-Ca showed a slight hypochromic effect and a new band at 300–350 nm, compared to PPHE-W. This is due to the complex compound with calcium ions, which modified the electronic distribution in the molecule [13,32,33].

Ti-CT and Ti-CT-CH were already physically and chemically characterized [34,35]. This paper is focused on the comparison of Ti-CT-CH-TPP and Ti-CT-CH-TPP-PPHE, which were observed by fluorescence microscopy to check for the effective functionalization of the CH coating with polyphenols. Pictures are reported in Fig. 2. The auto-fluorescence of polyphenols allowed us to verify their presence and uniform distribution on the surface of Ti-CT-CH-TPP-PPHE. The intensity of the fluorescence signal was high even using a detection time of 100 ms. Conversely, almost no signal was detected on Ti-CT-CH-TPP, even if the detection time was increased to 1000 ms.

XPS analyses were performed on Ti-CT-CH-TPP and Ti-CT-CH-TPP-PPHE. The survey chemical analyses are reported in Table 2, while the profile fitting of the C and O region is reported in Fig. 3. Ti-CT-CH-TPP was primarily composed of carbon, oxygen, and nitrogen, as expected

Table 1
Polyphenolic composition of the extract of Moscato Bianco seeds from unfermented grape seeds.

Moscato Bianco extract		mean ± st. dev.
GAE index (mg/g dw)[a]		540 ± 2.8
Total flavonoids (mg/g dw)		712 ± 1.5
$DPPH_{AAE}$ (mg/g dw)		15.2 ± 0.17
Gallic acid (mg/g dw)		3.12 ± 0.02
Condensed tannins (phloroglucinolysis)	Cond. tannins (mg/g dw)	340 ± 8.9
	mDP	4.4 ± 0.06
	% gallates	20.1 ± 0.07
	% EGC	nd
	% EC	79.6 ± 0.03
	% C	20.4 ± 0.03
Monomer, dimer, and trimer flavan-3-ols (mg/g dw)	C	15.93 ± 0.03
	EC	10.62 ± 0.28
	ECG	0.63 ± 0.00
	dimer B1	2.54 ± 0.01
	dimer B2	2.03 ± 0.13
	dimer B3	4.67 ± 0.01
	trimer C1	2.89 ± 0.05

[a] mg/g d.w. of freeze-dried extract.

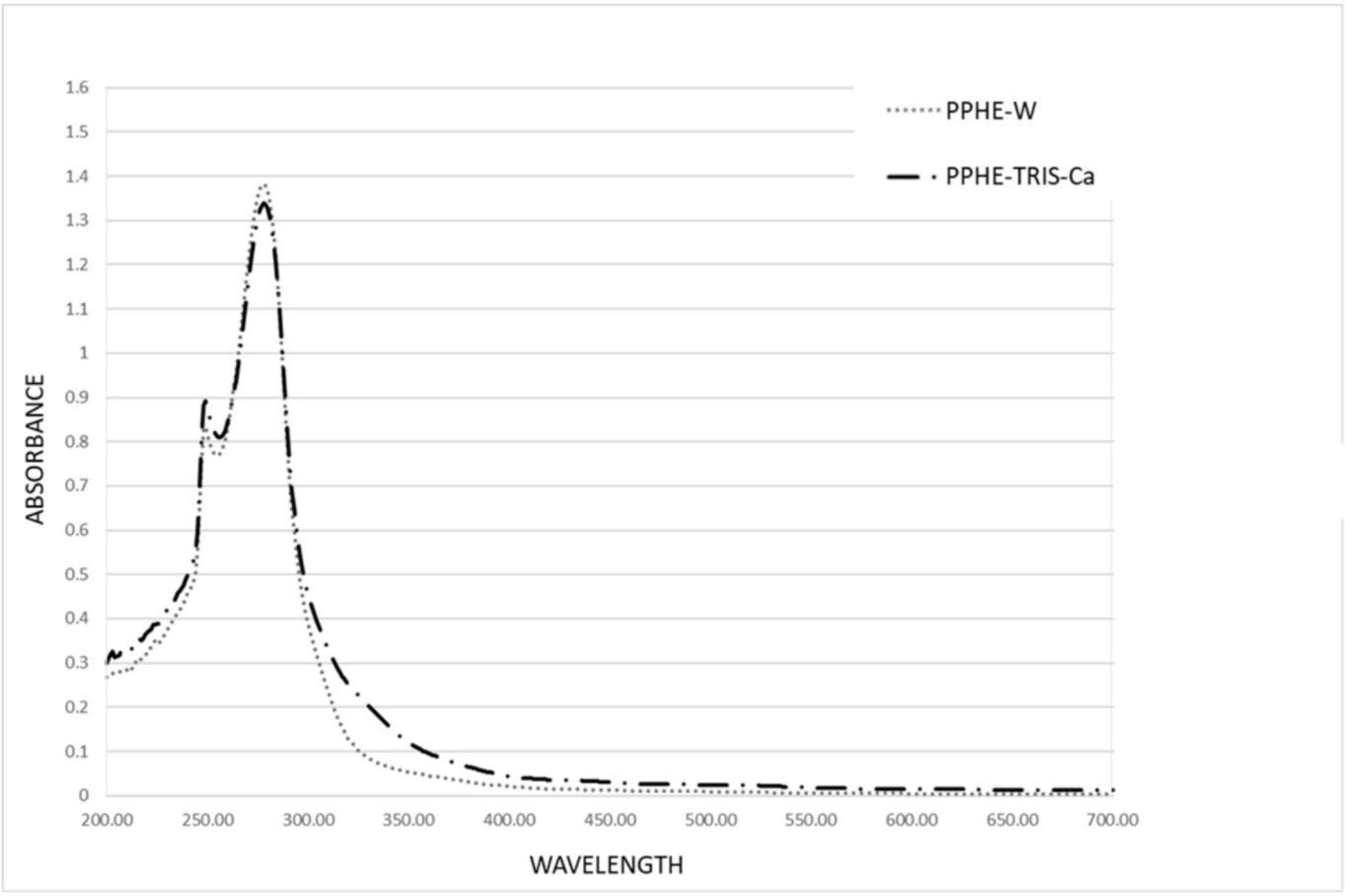

Fig. 1. Uv-Vis spectra of PPHE-TRIS-Ca and PPHE-W.

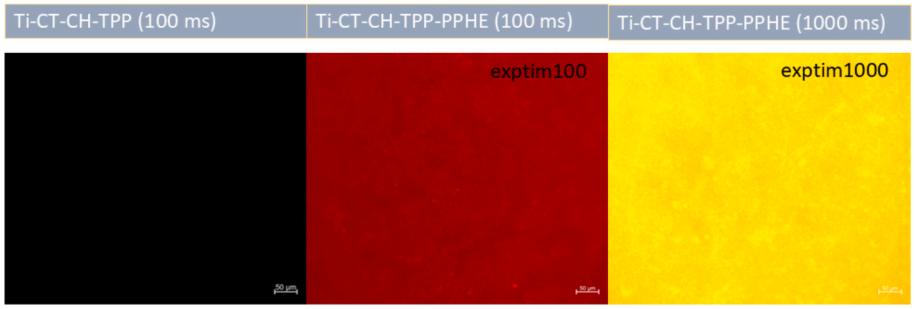

Fig. 2. Microscope fluorescence images of Ti-CT-CH-TPP (1000 ms) and Ti-CT-CH-TPP-PPHE (100 and 1000 ms).

Table 2
XPS survey analyses of Ti-CT-CH-TPP and Ti-CT-CH-TPP-PPHE.

	C 1s	O 1s	N 1s	P 1s	Ca 1s	Si 1s
Ti-CT-CH-TPP	61.5	30.0	4.3	1.3	–	2.9
Ti-CT-CH-TPP-PPHE	72.9	24.1	1.7	–	0.1	1.2

according to the chemical composition of CH, while phosphorus was due to the presence of TPP, which acts as a crosslinker. Silicon is a contaminant. The coating's thickness exceeded the penetration depth of the analysis, preventing the detection of the Ti substrate. Following the functionalization of the coating with polyphenols (Ti-CT-CH-TPP-PPHE), the detected percentages of oxygen and nitrogen decreased notably, and phosphorus was no longer present. These variations highlighted the presence of polyphenols and a reduced amount of CH (and TPP) on the surface. For a better understanding of surface chemistry, profile fitting of high-resolution spectra was analyzed. Before the functionalization with polyphenols (Ti-CT-CH-TPP), the high-resolution spectrum of the CH coating presented three peaks in the carbon region at 284.8, 286.4, and 288.1 eV (Fig. 3). The first peak is ascribed to C—C or C—H, while the second peak is ascribed to C–OH, C-O-C, and/or C—N, and the third peak is due to C═O (residual acetyl groups) [16,36,37]. On Ti-CT-CH-TPP-PPHE, three peaks at similar energy values were detected with a lower contribution of C═O.

In the oxygen region, the observed peaks on Ti-CT-CH-TPP are at 532.8 (COOH) and 531.4 (COO^-, C—O), which are related to CH with residual acetylation. Two minor peaks related to Ti oxide (529.9 eV - Ti—O) and OH acidic groups (530.9 - acOH) have very low areas, due to the higher thickness of the CH layer than the penetration depth of the beam. On Ti-CT-CH-TPP-PPHE, the same peaks were detected, plus a

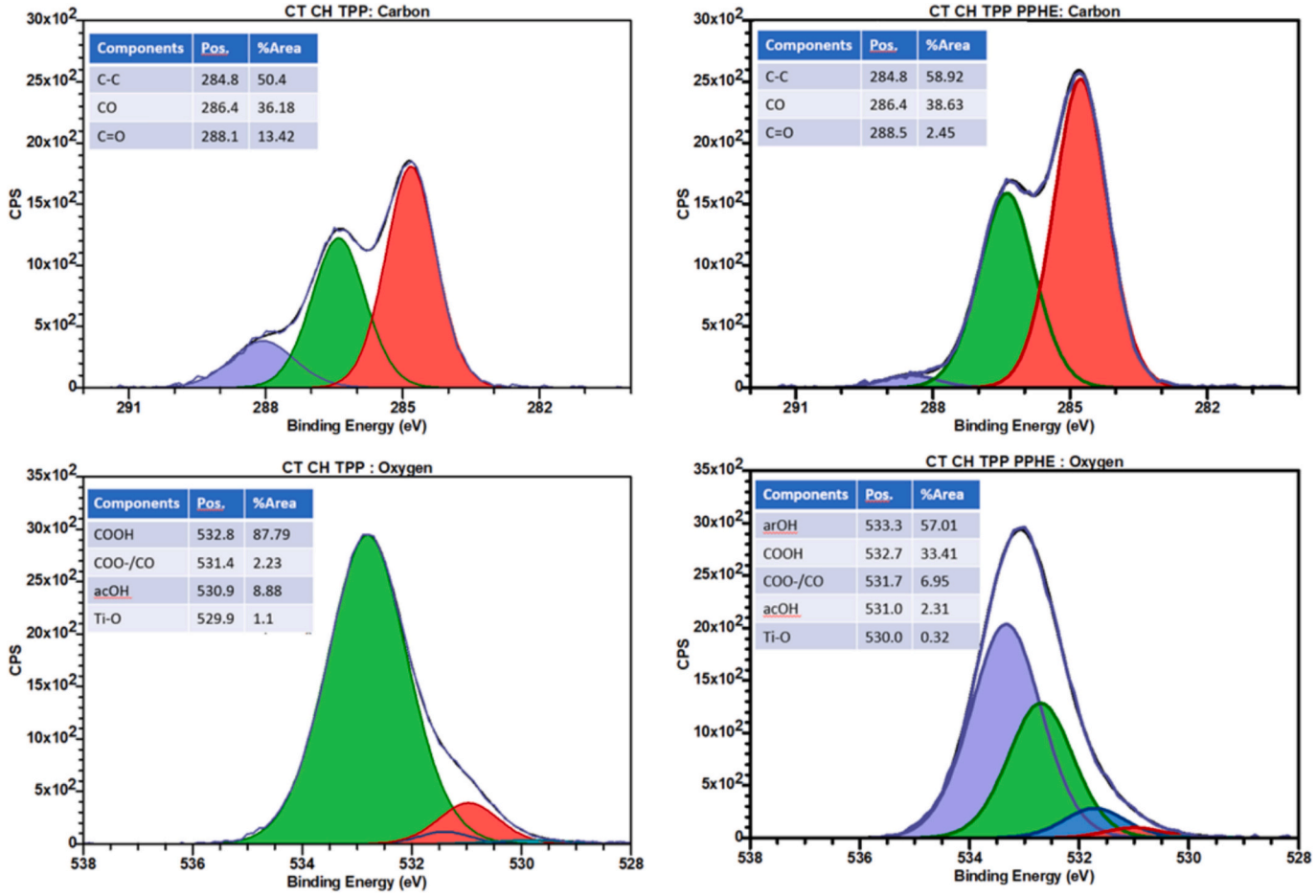

Fig. 3. Fitting of the carbon and oxygen regions in the high-resolution spectra of Ti-CT-CH-TPP-PPHE and Ti-CT-CH-TPP.

strong peak at 533.3 eV, which can be ascribed to phenolic OH groups (ArOH) typical of polyphenols [16,37].

3.2. Cytocompatibility studies

The cytocompatibility of the functionalized titanium surfaces was evaluated through a multi-faceted approach. We assessed cell metabolic activity via the resazurin reduction assay, cytotoxicity via the LDH release assay, and morphology via SEM analysis. The results collectively indicate that while the intermediate chitosan-based coatings inhibit cell adhesion, the final incorporation of the polyphenolic extract (PPHE) successfully restores it. The metabolic activity of hBM-MSC seeded on the Ti-CT-CH-TPP-PPHE disc was normalized towards the Ti-CT specimens that were considered as control (=100 % viability) due to the previous articles by the Authors showing comparable cytocompatibility with bulk Ti [34,38]. As shown in Fig. 4, the introduction of the chitosan layer, with or without TPP crosslinking (Ti-CT-CH and Ti-CT-CH-TPP), led to a significant decrease in metabolic activity of hBM-MSCs. This finding was also confirmed by the SEM images, which reveal significantly lower populated surfaces with cells exhibiting a rounded

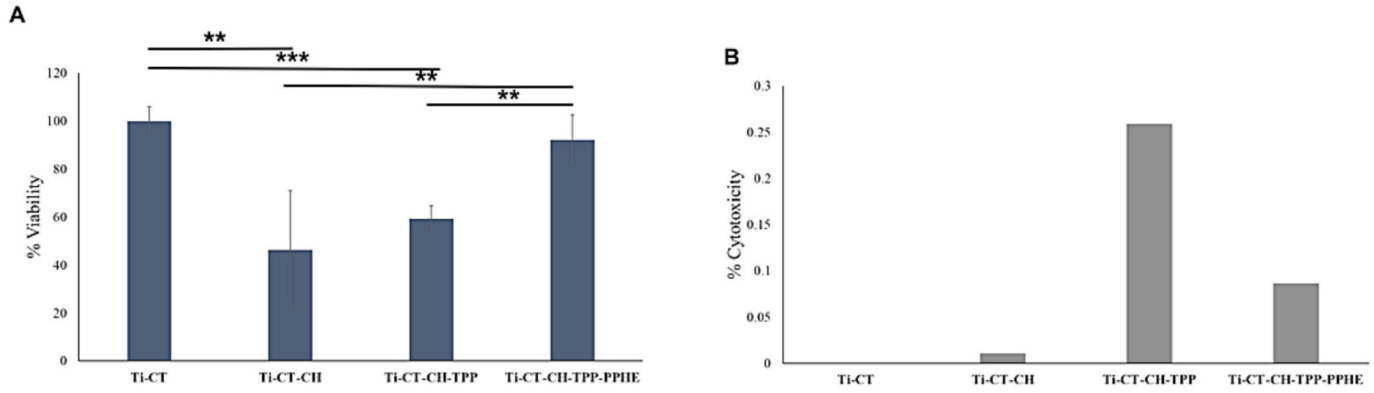

Fig. 4. Cytocompatibility of human bone marrow-derived mesenchymal stem cells (hBM-MSCs) cultured for 24 h on the surfaces of four titanium discs. (A) Percentage viability of hBM-MSCs normalized to Ti-CT (100 % viability) (**$p < 0.01$; ***$p < 0.001$). Bars represent mean values ± standard deviation of $n = 3$ biological replicates. (B) Percentage cytotoxicity, quantified by measuring the release of lactate dehydrogenase (LDH) as an indicator of cell membrane damage.

morphology, which can be indicative of poor attachment and spreading (Fig. 5). However, the LDH cytotoxicity assay (Fig. 4) showed that these surfaces are not cytotoxic, since the percentage of cytotoxicity for all samples was extremely low. These results may suggest that the observed reduction in viability is not due to the cytotoxic effects of the material on the cells, but that the chitosan-based substrates are anti-adhesive or cytostatic. Such surfaces prevent the cells from properly adhering, spreading, and proliferating.

On the other hand, we observed a dramatic reversal with the Ti-CT-CH-TPP-PPHE group. The addition of the polyphenolic extract restored the metabolic activity to a level comparable to the Ti-CT control (Fig. 4). This functional recovery was also confirmed by the SEM images (Fig. 5), where the cell layer was confluent and composed of elongated cells, similar to the control group.

3.3. Immunocompatibility study

The results of the immunocompatibility study performed on Ti-CT, Ti-CT-CH-TPP, and Ti-CT-CH-TPP-PPHE specimens using PBMCs are illustrated in Fig. 6. The introduction of the crosslinked CH coating (Ti-

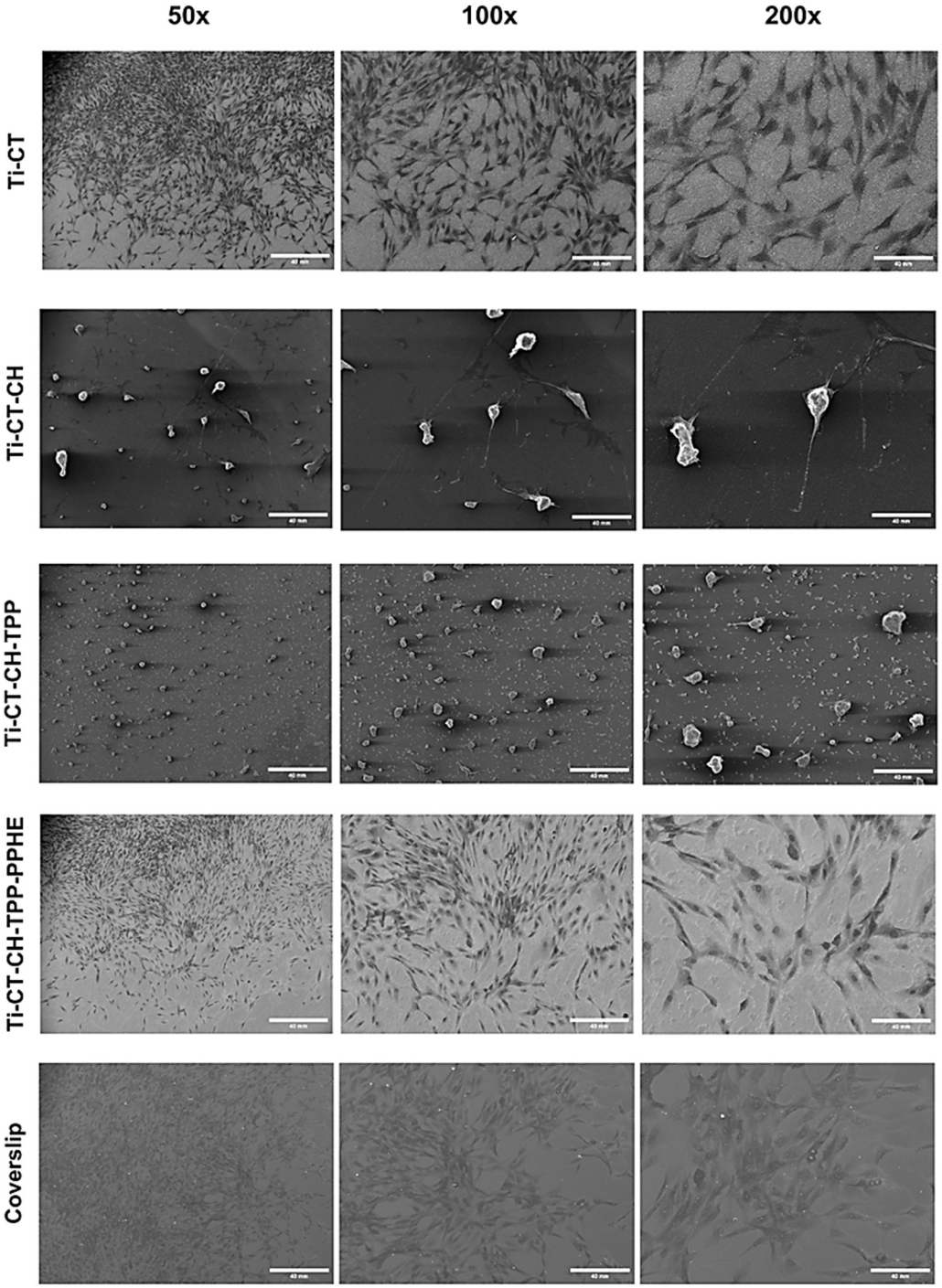

Fig. 5. Human bone marrow-derived mesenchymal stem cells (hBM-MSCs) morphology varies across different titanium surfaces. Representative scanning electron microscopy (SEM) images show the adhesion and spreading of hBM-MSCs after 24 h of culture on glass coverslip (control) and various titanium surfaces (Ti-CT, Ti-CT-CH, Ti-CT-CH-TPP, and Ti-CT-CH-TPP-PPHA). Images were taken at 50×, 100×, and 200× magnification. Scale bars = 40 μm.

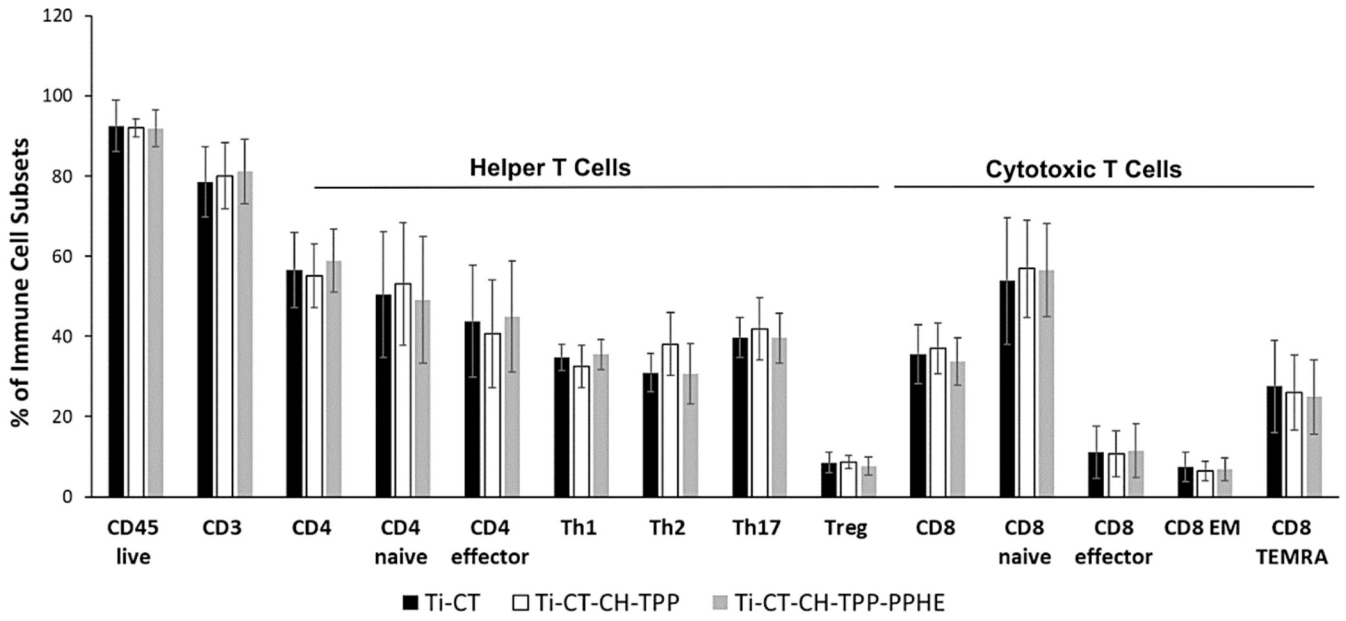

Fig. 6. Immunocompatibility using peripheral blood mononuclear cells cultured for 72 h in contact with Ti-CT, Ti-CT-CH-TPP, and Ti-CT-CH-TPP-PPHE titanium discs. Percentage of immune cell subsets following incubation with Ti-CT, Ti-CT-CH-TPP, and Ti-CT-CH-TPP-PPHE discs measured using BD FACSymphony™ A5. Bars represent the averages and error bars represent the standard deviations of the data from two independent experiments each with three healthy donors. T helper 1 (Th1) cells; T helper 2 (Th2) cells; T helper 17 (Th17) cells; regulatory T cells (Treg); CD8 effector memory cells (CD8 EM); effector memory cells re-expressing CD45RA (CD8 TEMRA). Bars represent mean values ± standard deviation of n = 6 biological replicates.

CT-CH-TPP) and the functionalization with the polyphenolic extract from white grape seeds (Ti-CT-CH-TPP-PPHE), did not induce changes in the immune cell subsets, confirming the immunocompatibility of the materials. Specifically, no significant differences were detected between the groups in the viability and/or number of CD4 cells, CD4 naïve cells, CD4 effector cells, T helper 1 (Th1) cells, T helper 17 (Th17) cells, regulatory T cells (Treg), CD8 cells, CD8 naïve cells, CD8 effector cells, CD8 effector memory cells (CD8 EM), and effector memory cells re-expressing CD45RA (CD8 TEMRA). Overall, the data indicate that the functionalized specimens (Ti-CT-CH-TPP-PPHE) do not disrupt the balance of immune cell populations.

3.4. Cellular proteomic studies

Two samples were selected for cellular proteomics analysis. Ti-CT was considered as the reference material due to the previous literature from the Authors showing its cytocompatibility [34,38,39]. Ti-CT-CH-TPP-PPHE was selected because polyphenols were the target of this omics study, mainly their effect on cells 'adaptation onto the specimens' surface. Unfortunately, it was not possible to include in this study a group representative for CH coating not functionalized with polyphenols (Ti-CT-CH or Ti-CT-CH-TPP) because the amount of collectable proteins was too low to be analyzed, due to the poor adhesion of the cells onto such substrates.

Results of the proteomics analysis are reported in Fig. 7. The principal component analysis (PCA) plot, representing the dataset reduced to the first two principal components, illustrated a significant spatial segregation of BM-MSCs cultured on the two distinct specimens, indicating differences in their overall phenotypic profiles. After 24 h of incubation, the proteomic profiling revealed significant differences in the expression of proteins by hBM-MSCs in contact with the polyphenol extract from white grape compared to those in contact with oxidized titanium surfaces (Ti-CT), as shown in Fig. 7A. In total, 86 proteins were significantly modulated, of which 48 were significantly downregulated and 38 were significantly upregulated in hBM-MSCs in contact with the polyphenol extract (Fig. 7B). The 50 most significant cellular proteins are represented in the hierarchical clustering heatmap in Fig. 7C, which shows a fluctuation in protein expression caused by the exposure of hBM-MSCs to the polyphenol extract.

To gain further insight into the functional implications of these differentially upregulated or downregulated expressed proteins, we performed GO enrichment analysis of the associated genes using DAVID, which categorized the GO terms into three distinct domains: biological processes (BP), cellular components (CC), and molecular functions (MF). The GO terms with a p-value ≤ 0.05 and associated with ≥ 3 genes were included for downregulated genes (Table 3) and upregulated genes (Table 4).

Our analysis revealed distinct functional profiles for the upregulated and downregulated protein sets. Specifically, upregulated proteins were significantly enriched in biological processes related to cytoplasmic translation, translation, intermediate filament organization, keratinization, and substantia nigra development (Table 4). Conversely, downregulated proteins showed significant enrichment in biological processes associated with protein folding, cytoplasmic translation, translation, translational elongation, and chaperone-mediated protein folding (Table 3). These findings suggest a potential shift towards increased protein synthesis and cytoskeletal remodeling.

Further supporting these observations, an analysis using the STRING database highlighted the significant upregulation of processes such as "cytoplasmic translation", "translation", "cellular macromolecule biosynthetic process", and "intermediate filament organization", as shown in Fig. 8.

3.5. Molecular proteomic studies

For molecular proteomics studies, fetal bovine serum (FBS) was selected as a rich source of proteins due to its large involvement in cell studies. Unlike the cellular proteomics test, all specimens were able to adsorb a sufficient amount of proteins from the seeded FBS to run omics experiments, therefore all the groups are reported here. The FBS proteins with altered adsorption to the functionalized specimens (Ti-CT-CH-TPP-PPHE) were considered for p-value <0.05 and fold change ≥ 1.5. Fig. 9 represents the proteins that significantly showed altered adsorption, both positive and negative.

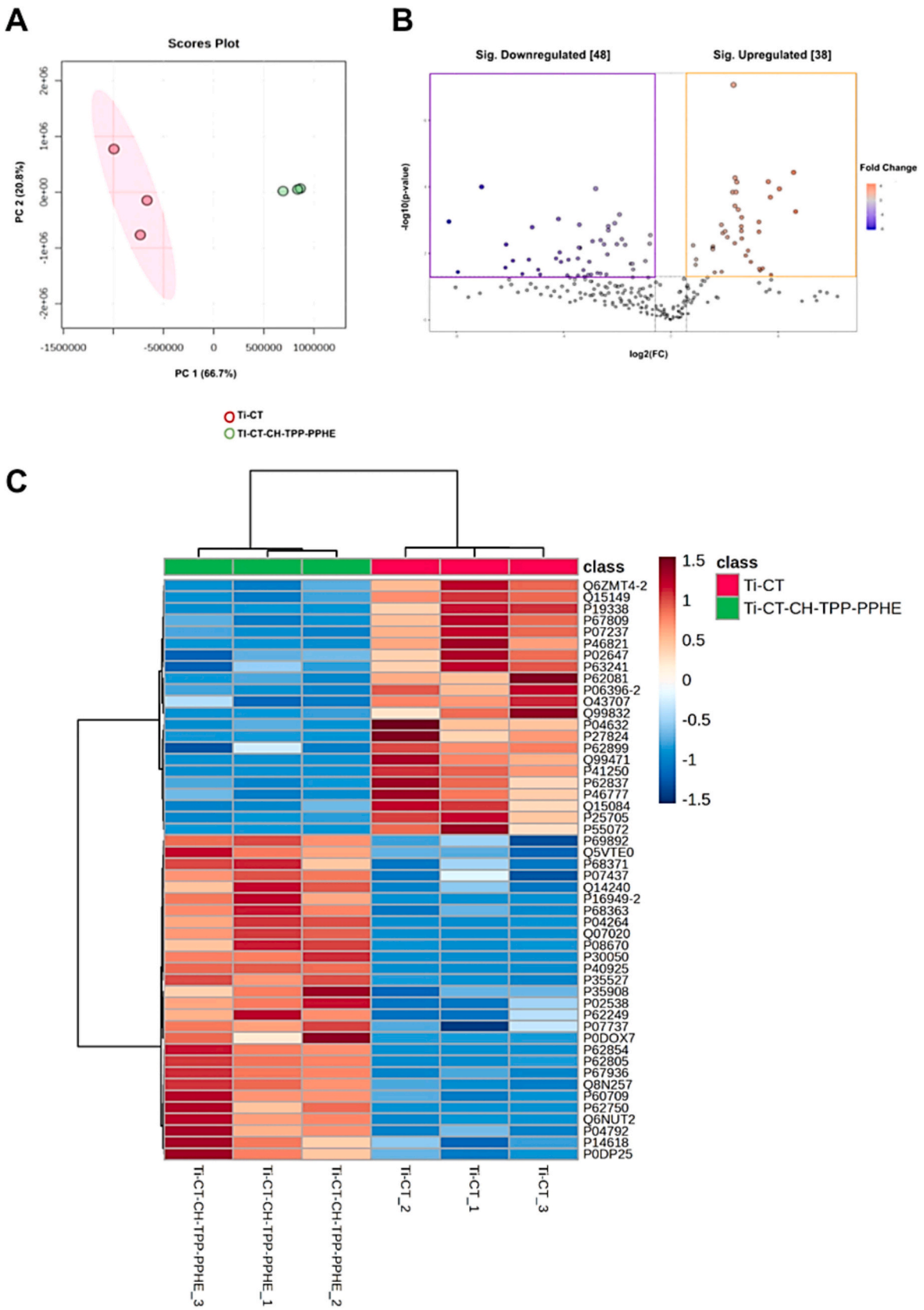

Fig. 7. Cellular protein profiling of human bone marrow-derived mesenchymal stem cells (hBM-MSCs) incubated for 24 h in contact with Ti-CT-CH-TPP-PPHE and Ti-CT ($n = 3$). (A) Principal components analysis (PCA) plot of the dataset reduced to two dimensions shows spatial separation between the hMSCs cultured on the two titanium discs. (B) The volcano plot revealed significant expression alterations for 48 proteins (38 upregulated and 48 downregulated) in hMSCs in contact with Ti samples coated with crosslinked CH functionalized with PPHE (Ti-CT-CH-TPP-PPHE) in comparison to those in contact with the oxidized (Ti-CT) titanium surfaces. (C) The heatmap shows the top 50 proteins with significant expression alterations. Samples are clustered by Pearson correlation and proteins by Euclidean distance.

Table 3
Table showing the top 5 Gene Ontology (GO) terms for Biological Process, Molecular Function, and Cellular Component categories identified from functional analysis of downregulated proteins using DAVID. Only terms with a *p*-value ≤0.05 and associated with ≥3 genes are included.

	GO number	GO term	p-value	Related proteins
Biological Process	GO:0002181	Cytoplasmic translation	1.63921E-07	Q07020, P62750, P30050, P62987, P62701, P62854, P62249
	GO:0006412	Translation	1.83478E-06	Q07020, P62750, P30050, Q5VTE0, P62987, P62701, P62854, P62249
	GO:0045109	Intermediate filament organization	4.58202E-05	P35527, P35908, P08670, P02538, P04264
	GO:0031424	Keratinization	0.001152505	P35908, Q86YZ3, P02538, P04264
	GO:0021762	Substantia nigra development	0.007334874	P60709, P00338, P0DP25
Cellular Component	GO:0070062	Extracellular exosome	3.08458E-33	P14618, Q5VTE0, P40925, P62750, P23528, P30050, P04264, P62854, P07437, P35527, P35908, Q86YZ3, P62805, Q9BTM1, P07737, P60709, P68371, P08670, P0C0S8, P00338, P02538, P62987, P62701, P04792, P67936, P21796, P62249
	GO:0000786	Nucleosome	1.76471E-32	P62805, P0C0S8, Q9BTM1, P60709, Q8N257
	GO:0005634	Nucleus	3.1551E-13	P14618, Q5VTE0, P62750, P23528, Q01105, P04264, Q07020, P07437, P35527, P35908, Q86YZ3, P62805, Q9BTM1, P07737, P60709, P0DP25, P68371, P0C0S8, P00338, P02538, P62987, Q6NUT2, P04792, Q8N257, P21796
	GO:0032991	Protein-containing complex	5.06234E-13	P07437, P62805, P60709, P0DP25, Q01105
	GO:0005576	Extracellular region	1.98215E-07	P07437, P0DOX7, P14618, Q86YZ3, P62805, P0DP25, P04264, P68371
Molecular Function	GO:0030527	Structural constituent of chromatin	1.03756E-32	P62805, P0C0S8, Q9BTM1, Q8N257
	GO:0046982	Protein heterodimerization activity	2.42852E-24	P62805, P0C0S8, Q9BTM1, P04264, Q8N257, P67936
	GO:0003723	RNA binding	4.33221E-14	Q07020, P62750, P14618, P62805, P08670, P07737, P30050, P62701, Q14240, P04792, P62249, P62854
	GO:0003677	DNA binding	8.3189E-12	P62805, P0C0S8, Q9BTM1, Q01105, Q8N257
	GO:0005200	Structural constituent of cytoskeleton	1.56684E-08	P07437, P35527, P35908, P08670, P60709, P02538, P68363, P68371

Table 4
Table showing the top 5 Gene Ontology (GO) terms for Biological Process, Molecular Function, and Cellular Component categories identified from functional analysis of upregulated proteins using DAVID. Only terms with a p-value ≤0.05 and associated with ≥3 genes are included.

	GO number	GO term	p-value	Related proteins
Biological Process	GO:0006457	Protein folding	8.18964E-08	Q99832, P17987, Q15084, P78371, Q99471, P27824, P61604, P07237
	GO:0002181	Cytoplasmic translation	1.58515E-06	P15880, P62899, P62081, P46777, P18621, P39019
	GO:0006412	Translation	7.18632E-06	P15880, P68104, P62899, P62081, P46777, P18621, P39019
	GO:0006414	Translational elongation	7.50849E-06	P26641, P68104, P63241
	GO:0061077	Chaperone-mediated protein folding	0.000117188	Q99832, P17987, P78371, Q99471
Cellular Component	GO:0070062	Extracellular exosome	8.00133E-27	P04632, P26641, P62837, P67809, P39019, P17987, Q15084, P25705, P07195, P41250, P02647, P62899, P78371, P27824, P61604, P55072, P60953, P07237, Q07065, Q14974, P06702, Q15149, P32119, P07339, P07858, Q09666, Q99832, P19338, O43707, P15880, P60660, P68104, P08133, P46777, Q16881
	GO:0005829	Cytosol	1.46021E-13	P04632, P26641, P62837, P67809, P62081, Q99471, P18621, P39019, P17987, Q15084, P63241, Q99584, P07195, P41250, P02647, P62899, P78371, P46821, P55072, P60953, P07237, Q00839, Q14974, P06702, Q15149, P32119, P07339, Q09666, Q99832, P15880, P60660, P68104, P46777, Q16881
	GO:0005925	Focal adhesion	1.45426E-08	Q15149, O43707, P15880, P62899, P62081, Q09666, P08133, P46777, P60953, P07237, P39019
	GO:0022626	Cytosolic ribosome	4.55215E-08	P15880, P68104, P62899, P62081, P46777, P18621, P39019
	GO:0005737	Cytoplasm	6.47587E-07	P04632, P26641, P67809, P62081, Q99471, P18621, P39019, P25705, P63241, Q99584, P07195, P41250, P62899, P55072, P60953, Q07065, Q14974, P06702, Q15149, P32119, Q09666, Q99832, O43707, P15880, P68104, P08133, P46777, Q16881
Molecular Function	GO:0003723	RNA binding	5.48146E-14	Q07065, Q14974, Q15149, P67809, P62081, Q09666, P18621, P39019, P19338, P17987, P15880, O43707, P25705, P68104, P63241, P62899, P27824, P61604, P46777, P55072, P07237, Q00839
	GO:0005515	Protein binding	8.06466E-06	P04632, P26641, P62837, P67809, P62081, Q99471, P18621, P39019, P17987, Q15084, P25705, P63241, Q99584, P07195, P41250, P02647, P62899, P78371, P27824, P61604, P46821, P55072, P60953, P07237, Q00839, Q07065, Q14974, P06702, Q15149, P32119, P07339, P07858, Q09666, Q99832, P19338, O43707, P15880, P60660, P68104, P08133, P46777, Q16881
	GO:0051082	Unfolded protein binding	9.91482E-06	Q99832, P17987, P78371, Q99471, P27824, P61604
	GO:0003746	Translation elongation factor activity	4.95374E-05	P26641, P68104, P63241
	GO:0003735	Structural constituent of ribosome	6.06236E-05	P15880, P62899, P62081, P46777, P18621, P39019

To gain further insight into the functional implications of the FBS proteins, the associated genes underwent GO enrichment analysis using DAVID. The GO terms were categorized into three distinct domains: BP, CC, and MF. The GO terms with a *p*-value ≤0.05 were included for proteins whose adsorption was positively altered (Table 5). However, processing the proteins whose adsorption was negatively altered did not result in an outcome with GO terms. The proteins with positive adsorption were significantly enriched in biological processes related to negative regulation of endopeptidase activity, immunoglobulin production involved in immunoglobulin-mediated immune response, antigen processing and presentation of peptide antigen via MHC class I, positive regulation of immune response, and peptide antigen assembly

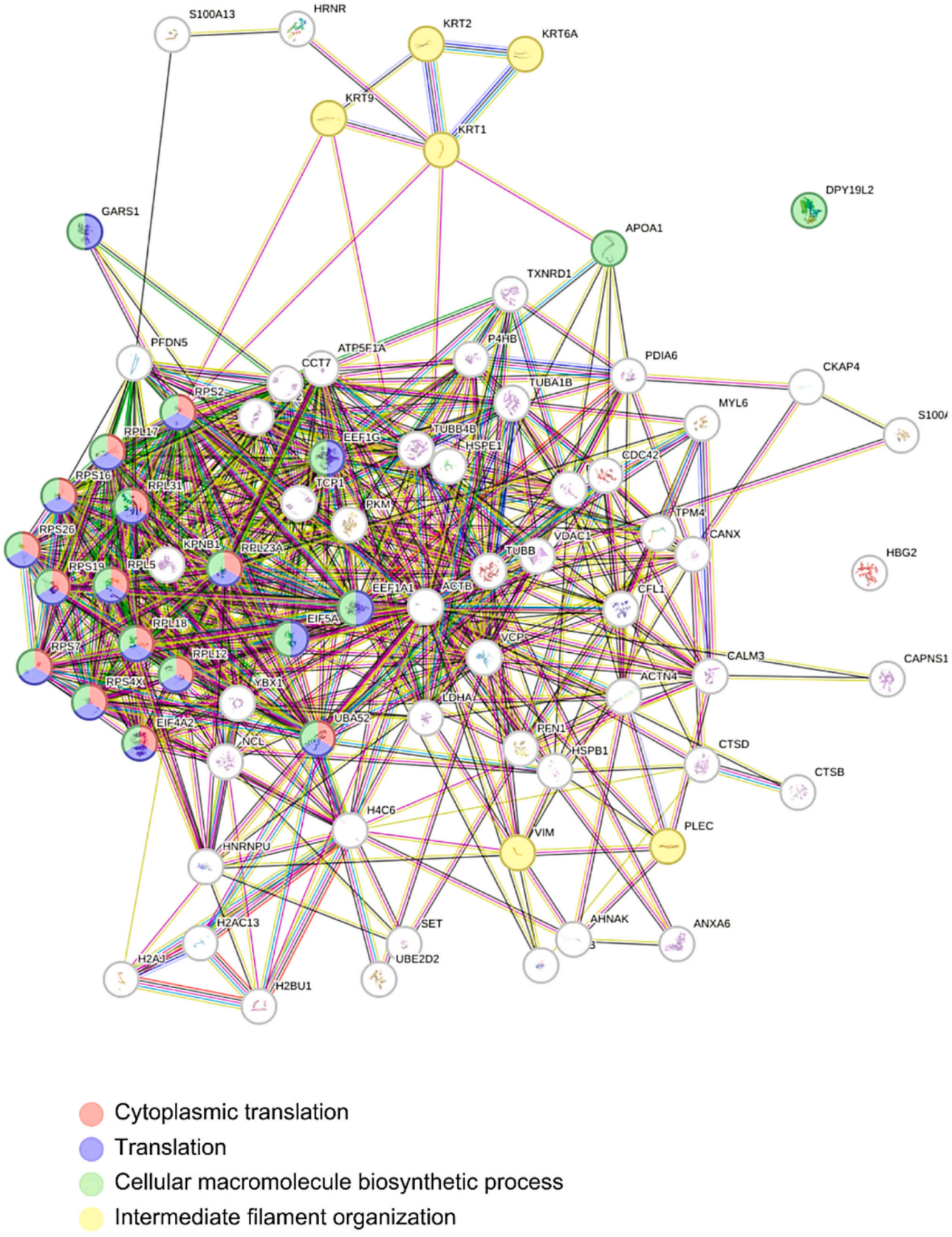

Fig. 8. Gene Ontology (GO) enrichment analysis of the differentially expressed proteins (downregulated and upregulated) using STRING database with the top 4 biological processes highlighted (n = 3).

A

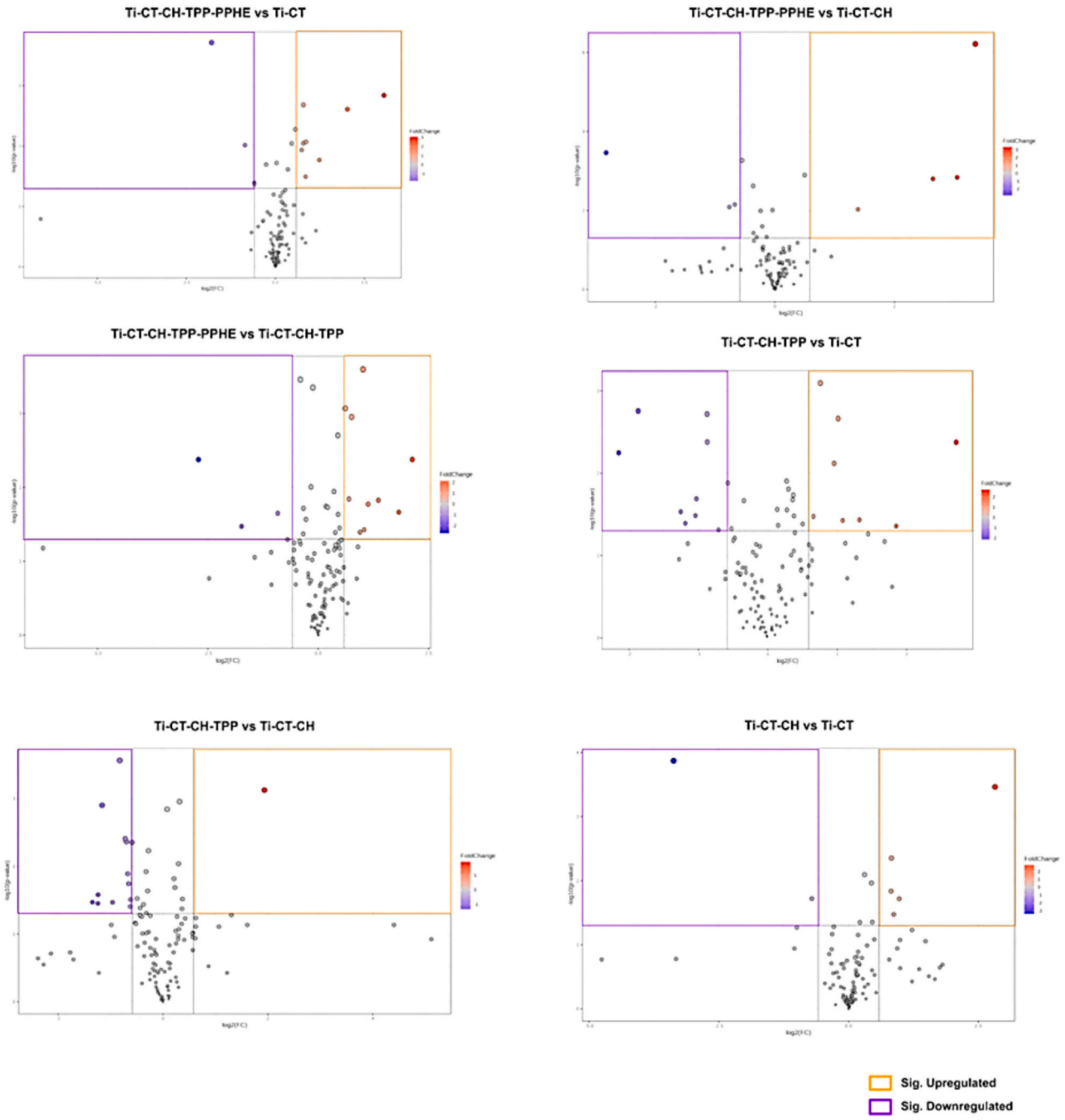

B

	Ti-CT-CH-TPP-PPHE vs Ti-CT	Ti-CT-CH-TPP-PPHE vs Ti-CT-CH	Ti-CT-CH-TPP-PPHE vs Ti-CT-CH-TPP	Ti-CT-CH-TPP vs Ti-CT	Ti-CT-CH-TPP vs Ti-CT-CH	Ti-CT-CH vs Ti-CT
Sig. Positive Adsorption	8	4	10	8	1	5
Sig. Negative Adsorption	4	3	3	9	13	2

Fig. 9. Molecular protein profiling of fetal bovine serum (FBS) proteins following incubation for 2 h in contact with Ti-CT, Ti-CT-CH, Ti-CT-CH-TPP, and Ti-CT-CH-TPP-PPHE ($n = 3$). (A) The volcano plots reveal significant affinity alterations for FBS proteins for all the titanium surfaces. (B) The number of significantly upregulated and downregulated FBS proteins for all the titanium surfaces.

Table 5
Table showing the top 5 Gene Ontology (GO) terms for Biological Process, Molecular Function, and Cellular Component categories identified from functional analysis of fetal bovine serum (FBS) proteins exhibiting positive adsorption using DAVID. Only terms with a p-value ≤0.05 are included.

	GO number	GO term	p-value	Related proteins
Biological Process	GO:0010951	Negative regulation of endopeptidase activity	0.000172832	A2I7N3, A2I7N0, A6QPQ2
	GO:0002381	Immunoglobulin production involved in immunoglobulin-mediated immune response	0.008308756	P01888
	GO:0002474	Antigen processing and presentation of peptide antigen via MHC class I	0.010624576	P01888
	GO:0050778	Positive regulation of immune response	0.010955028	P01888
	GO:000250	Peptide antigen assembly with MHC class II protein complex	0.012275893	P01888
Cellular Component	GO:0042583	Chromaffin granule	1.89971E-08	A2I7N3, A2I7N0, A6QPQ2, A2I7N2
	GO:0031410	Cytoplasmic vesicle	3.40365E-05	A2I7N3, A2I7N0, A6QPQ2, A2I7N2
	GO:0005615	Extracellular space	5.81048E-05	Q2KIG3, A2I7N3, A2I7N0, A6QPQ2, A2I7N2, P02465
	GO:0042612	MHC class I protein complex	0.012166359	P01888
	GO:0042613	MHC class II protein complex	0.015618584	P01888
Molecular Function	GO:0004867	Serine-type endopeptidase inhibitor activity	2.66783E-05	A2I7N3, A2I7N0, A6QPQ2, A2I7N2
	GO:0023026	MHC class II protein complex binding	0.014440528	P01888
	GO:0042605	Peptide antigen binding	0.020465949	P01888

with MHC class II protein complex (Table 5).

Using the STRING database, the analysis of all FBS proteins with positively altered adsorption to Ti-CT-CH-TPP-PPHE in comparison to Ti-CT did not reveal significant correlations. Moreover, the analysis suggested that the FBS proteins with positively altered adsorption are mainly cellular components related to "chromaffin granule" and "extracellular space", as shown in Fig. 10.

3.6. Antibacterial activity

The antibacterial properties against *S. aureus* were evaluated using SEM analysis and 3D rendering by SEM software. As shown in Supplementary Fig. 1, the bacteria were able to adhere to the surfaces of all specimens and form biofilms, suggesting that CH and the polyphenolic extract from white grape seeds were not effective in preventing biofilm formation onto specimens' surface.

3.7. Outlier analysis

Normalized peak areas were log-transformed to handle the range of peak intensities and to stabilize the variance. The initial situation and data distributions for each sample type and biomaterial are in Fig. 11.

The probability density functions in Fig. 11 of BM-MSC proteins depict the presence of a majority of overexpressed proteins, following a quasi-normal distribution with different characteristics in the two conditions. On the other hand, the curves look bimodal and close to each other for FBS proteins. Fig. 11 confirms the distinct expression and lack of overlap between BM-MSC proteins and FBS proteins. Consequently, FBS proteins and BM-MSC proteins expression levels could be analyzed separately in the next steps of analysis.

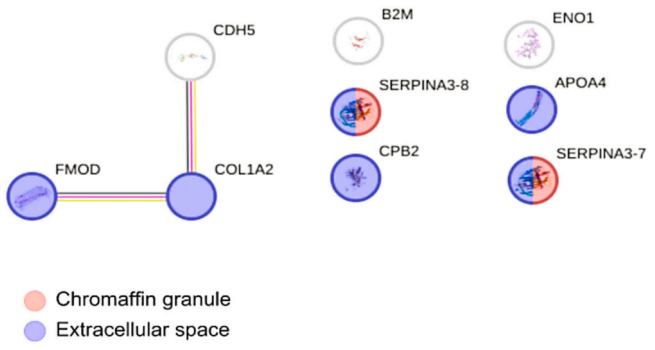

Fig. 10. Gene Ontology (GO) enrichment analysis of fetal bovine serum (FBS) proteins exhibiting positive adsorption using STRING database with the top 2 cellular components highlighted (n = 3).

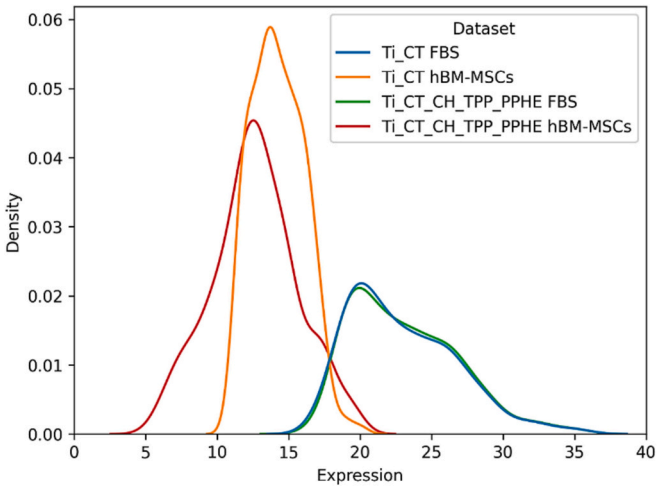

Fig. 11. Probability density estimation of log-transformed peak areas for human bone marrow-derived mesenchymal stem cells (hBM-MSCs) proteins and fetal bovine serum (FBS) proteomics data.

3.7.1. Outliers identification

In proteomics, nonlinear low-dimensional embeddings can provide a more accurate overall picture of how the different conditions relate to each other, showing both local clustering and global patterns, such as how similar or different one cell line or treatment group is from another. UMAP 2D representations were created for the FBS proteins and BM-MSC proteins groups separately, starting from the log-transformed expression values of the three samples (Fig. 12A). The goal was to identify outliers and analyze proteins (and related genes) with abnormal expression within species. Isolation Forest, an unsupervised machine learning algorithm for anomaly detection, defined the outliers as shown in Fig. 12A. The outlier genes for each biomaterial are in Fig. 12B and Fig. 12C, for BM-MSC proteins and FBS proteins, respectively, as Venn diagrams. Whereas BM-MSC data have more specific genes active for Ti-CT-CH-TPP-PPHE than Ti-CT, there are smaller sets and more shared genes in FBS data.

3.7.2. Functional profiling of the outliers

All outliers of the BM-MSC proteins were retained for GO and functional analysis. Indeed, outlier genes can indicate potential biomarkers for experimental conditions or could be involved in specific pathways for a biomaterial. Table 6 refers to chemically treated titanium (Ti-CT), while Table 7 to functionalized titanium (Ti-CT-CH-TPP-PPHE) and contains only values below statistical significance.

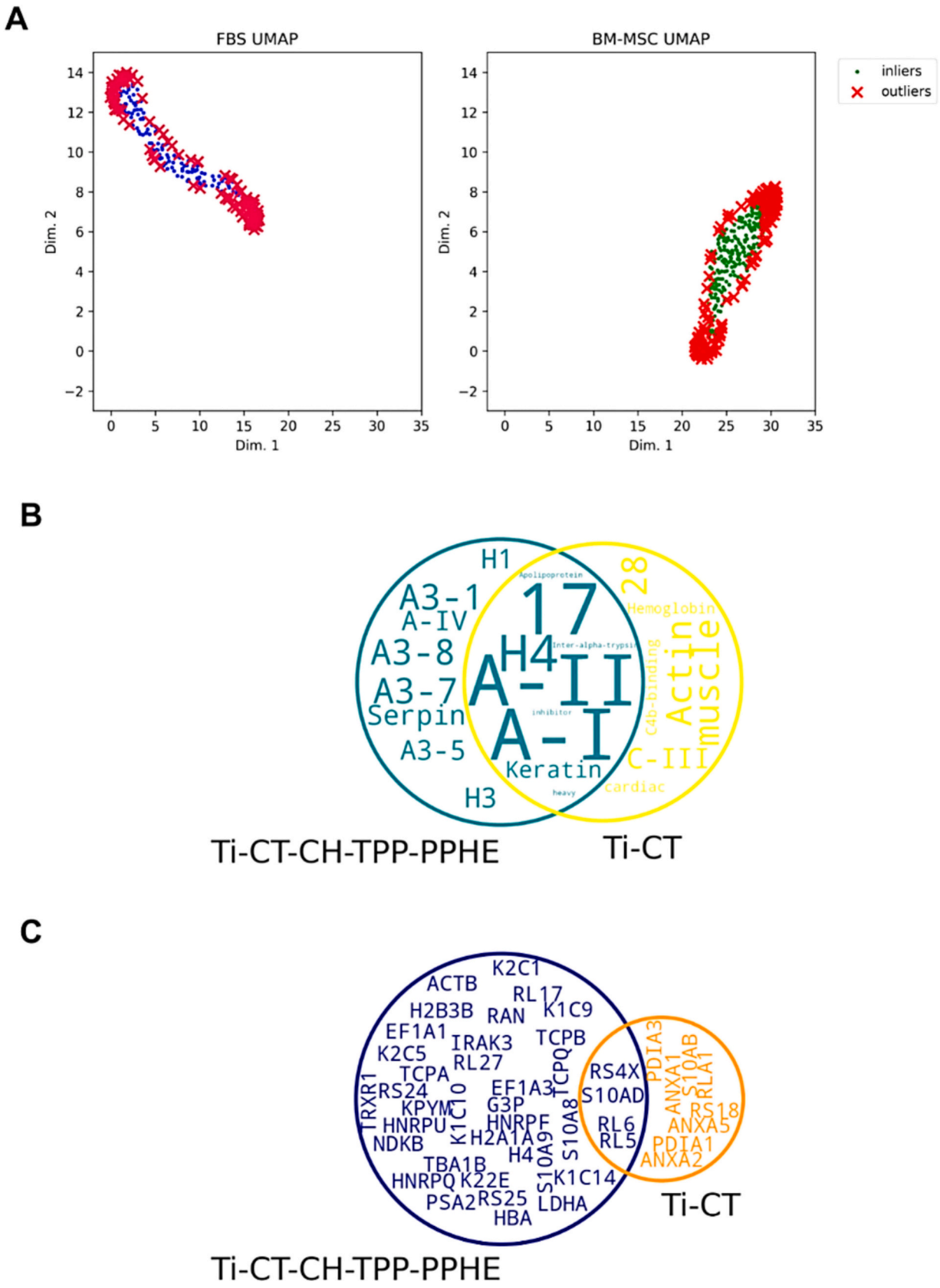

Fig. 12. Outliers identification. (A) Outliers on FBS and BM-MSC proteins from UMAP low dimensional embeddings through Isolation Forest. (B) Venn diagram showing common outlier genes across experimental condition using BM-MSC proteins. (C) Venn diagram showing common outlier genes across experimental conditions using FBS proteins.

Table 6
Functional profiling of outliers' gene on TI-CT for BM-MSC proteins.

Source	Description
GO:BP	negative regulation of coagulation
GO:BP	plasma membrane repair
GO:CC	extracellular matrix
GO:CC	collagen-containing extracellular matrix
GO:CC	external encapsulating structure
GO:CC	zymogen granule membrane
GO:CC	zymogen granule
GO:MF	phospholipase inhibitor activity
GO:MF	modified amino acid binding
GO:MF	phosphatidylserine binding
GO:MF	phospholipid binding
GO:MF	calcium-dependent protein binding
GO:MF	lipase inhibitor activity
GO:MF	calcium-dependent phospholipid binding
WP	Prostaglandin synthesis and regulation

Among the bioactivities identified by the analysis, several GO terms and pathways point towards specific cellular processes and molecular functions potentially influenced by the Ti-CT surface. In terms of biological processes (GO:BP), "plasma membrane repair" was identified. Regarding cellular components (GO:CC), the analysis highlighted terms associated with the "extracellular matrix", specifically the "collagen-containing extracellular matrix", as well as the "external encapsulating structure". Furthermore, terms related to secretory granules, such as the "zymogen granule membrane" and "zymogen granule", were also present. On the level of molecular functions (GO:MF), several binding and inhibitory activities were indicated. These include "phospholipase inhibitor activity", "modified amino acid binding", "phosphatidylserine binding", "phospholipid binding", "calcium-dependent protein binding", "lipase inhibitor activity", and "calcium-dependent phospholipid binding". Finally, pathway analysis revealed potential involvement in "prostaglandin synthesis and regulation" (WP).

For the Ti-CT-CH-TPP-PPHE samples, the analysis revealed several enriched bioactivities. In terms of biological processes (GO:BP), the analysis highlighted terms related to "vesicle fusion", specifically its positive regulation and overall regulation. Additionally, "wound healing" emerged as a potentially relevant biological process influenced by this surface modification. Regarding cellular components (GO:CC), several terms associated with cell-cell interactions and the extracellular environment were identified. These include "anchoring junction", "extracellular region", "cytosol", "extracellular exosome", "adherens junction", "extracellular vesicle", "extracellular membrane-bounded organelle", and "extracellular organelle". On the level of molecular functions (GO:MF), the analysis pointed towards activities involved in cell adhesion, such as "cell-cell adhesion mediator activity" and "cell adhesion molecule binding". Specifically, "cadherin binding" involved in cell-cell adhesion and general cadherin binding were also noted. Furthermore, similar to the Ti-CT samples, "phospholipase inhibitor activity", "phospholipase A2 inhibitor activity", "calcium-dependent phospholipid binding", "lipase inhibitor activity", and "phosphatidylserine binding" were identified. Transcription factor (TF) analysis indicated potential regulation by Fra-1 (motif: TGACTCAN), JUNB:C-JUN (motif: NATGACKCAT), and the complex C-JUN:FRA-1 (motif: NNATGACTCATNN), all with a high match class (1). Finally, pathway analysis revealed an association with "prostaglandin synthesis and regulation" (WP), a pathway also observed in the Ti-CT samples.

3.7.3. Ortholog outliers' identification

Cross-species gene expression analysis involves comparing gene expression data from different species to identify evolutionary conserved transcriptional responses. Orthologs are genes in other species that originated from a common ancestral gene and evolved due to *speciation events* (when a species diverges into two or more distinct species). The input genes were bovine, and the target organisms were humans. Orthologous genes are reported in Table 8. Among the identified human orthologs, only three were found to be outliers across the experimental conditions when considering FBS proteins (Table 9).

Specifically, Peroxiredoxin 2 (PRDX2) and Apolipoprotein A-I (APOA1) were identified as outlier orthologs in human BM-MSCs exposed to the Ti-CT-CH-TPP-PPHE surface, suggesting a potentially conserved and significant response to this specific biomaterial modification in human cells. In contrast, Lactate Dehydrogenase B (LDHB) did not emerge as an outlier in human BM-MSCs for either Ti-CT or Ti-CT-CH-TPP-PPHE conditions. Interestingly, APOA1 was also identified as an outlier when considering FBS proteins alone, regardless of the surface modification. This suggests that APOA1 expression might be particularly sensitive to the presence of FBS proteins in both experimental groups.

4. Discussion

The extract used in this paper (PPHE) comes from only unfermented seeds of a white grape (Moscato Bianco cultivar). This extract is expected to be distinguished from the extracts of other cultivars [20], such as the Barbera grape pomace used in previous studies [13,16,24,40], which contained fermented skins and seeds from a black grape. The high polyphenolic content of PPHE is due to the higher natural concentration of the seeds of the Moscato Bianco cultivar and the winemaking process from which it comes, in which grape pomace is separated from the must before alcoholic fermentation and does not undergo polyphenol losses due to maceration. As expected, PPHE had a flavonoid fraction constituted only by flavanols (condensed tannins and monomeric flavan-3-ols – Table 1) without anthocyanins, typical of the skins of black grapes as in

Table 7
Functional profiling of outliers' gene on TI-CT-CH-TPP-PPHE for BM-MSC proteins.

Source	Description
GO:BP	positive regulation of vesicle fusion
GO:BP	regulation of protein binding
GO:BP	wound healing
GO:BP	regulation of vesicle fusion
GO:CC	anchoring junction
GO:CC	extracellular region
GO:CC	cytosol
GO:CC	extracellular exosome
GO:CC	adherens junction
GO:CC	extracellular vesicle
GO:CC	extracellular membrane-bounded organelle
GO:CC	extracellular organelle
GO:MF	cell-cell adhesion mediator activity
GO:MF	cell adhesion molecule binding
GO:MF	phospholipase inhibitor activity
GO:MF	cadherin binding involved in cell-cell adhesion
GO:MF	cadherin binding
GO:MF	phospholipase A2 inhibitor activity
GO:MF	calcium-dependent phospholipid binding
GO:MF	lipase inhibitor activity
GO:MF	phosphatidylserine binding
TF	Factor: Fra-1; motif: TGACTCAN; match class: 1
TF	Factor: JUNB:C-JUN; motif: NATGACKCAT; match class: 1
TF	Factor: C-JUN:FRA-1; motif: NNATGACTCATNN; match class: 1
WP	Prostaglandin synthesis and regulation

fermented Barbera grape pomace, and flavonols (e.g. quercetin, myricetin). This is of interest because flavanols are generally considered the most biologically active polyphenols as anti-inflammatory agents, especially in models of chronic inflammation and conditions where oxidative stress plays a significant role [41,42]. Moreover, this class of polyphenols is known for its ability to promote osteogenesis and reduce osteoclastogenesis [43–45]. In conclusion, this polyphenolic extract has greater potential than others in terms of biological activity.

The DLS results confirmed the effectiveness of the protocol for preparing the solution used for the functionalization (PPHE-TRIS-Ca) to get a homogeneous colloidal suspension of polyphenols.

The zeta potential values of the extract in solutions with or without the addition of Ca^{2+} ions evidenced that the presence of calcium ions in the functionalization solution made the zeta potential less negative, because of the formation of a complex compound of polyphenols with the calcium ions and the neutralization of some hydroxyl groups that would otherwise be negatively charged. The presence of this complex compound in the functionalization solution was confirmed by UV–Vis spectroscopy and, as expected, allowed a larger solubility of polyphenols with a greater value of antioxidant activity (GAE). In conclusion, the antioxidant activity of the used functionalization solution was about 3 times that of a similar solution prepared with a Barbera extract [13], confirming expectations.

This extract allowed an efficient and uniform functionalization of the CH coating on Ti-CT-CH-PPP-PPHE, as revealed by fluorescence microscopy and XPS analysis. The reduction in the oxygen and nitrogen contents and the disappearance of the signal of phosphorus agree with the different chemical compositions of CH and polyphenols [16]. The appearance of a strong contribution due to phenolic OH groups in the oxygen region also confirmed the effective functionalization. XPS also evidenced residual acetyl groups on the CH layer.

Concerning the coating stability and release of polyphenols, it was evidenced in a previous paper [16] a difference in the kinetics of the release of the polyphenols by a similar coating in different chemical environments, with a “smart” and larger release of polyphenols in a solution mimicking the inflammatory conditions. The simulated inflammatory solution caused a larger swelling of chitosan, which led to a much more porous appearance. The coating released a minimum quantity of polyphenols in PBS in the first 24 h.

The first step in the biological evaluation of novel biomaterials is to test their cytocompatibility to confirm their ability to interact with living cells without causing any adverse effects. In our study, we illustrated that CH did not induce cytotoxicity to the hBM-MSCs as results were comparable to the bulk Ti-CT control that was demonstrated to be cytocompatible in previous literature [34,38,39]; however, the CH surface was not cell-friendly, preventing a strong and permanent cellular adhesion and spread. Conversely, adding the polyphenolic extract was shown to significantly increase the cells' metabolic activity, thus significantly improving the affinity at the interface with cells. Previous authors were also able to verify the effects of polyphenols on the

Table 8
Genes in different species that originated from a common ancestor.

Bovine gene	Converted ID	Canonical Ensembl ID	Human gene	Description
THRB	ENSBTAG00000017802	ENSG00000151090	THRB	thyroid hormone receptor beta
AMBP	ENSBTAG00000060375	ENSG00000106927	AMBP	alpha-1-microglobulin/bikunin precursor
KNG1	ENSBTAG00000005122	ENSG00000113889	KNG1	kininogen 1
HBA	ENSBTAG00000051412	ENSG00000188536	HBA2	hemoglobin subunit alpha 2
HBA	ENSBTAG00000051412	ENSG00000206172	HBA1	hemoglobin subunit alpha 1
APOA1	ENSBTAG00000065859	ENSG00000118137	APOA1	apolipoprotein A1
APOH	ENSBTAG00000001915	ENSG00000091583	APOH	apolipoprotein H
APOC3	ENSBTAG00000012398	ENSG00000110245	APOC3	apolipoprotein C3
COMP	ENSBTAG00000004630	ENSG00000105664	COMP	cartilage oligomeric matrix protein
CL43	ENSBTAG00000047317	ENSG00000133661	SFTPD	surfactant protein D
ITIH3	ENSBTAG00000007846	ENSG00000162267	ITIH3	inter-alpha-trypsin inhibitor heavy chain 3
RAP1B	ENSBTAG00000008967	ENSG00000127314	RAP1B	RAP1B, member of RAS oncogene family
APOA2	ENSBTAG00000009212	ENSG00000158874	APOA2	apolipoprotein A2
APOE	ENSBTAG00000010123	ENSG00000130203	APOE	apolipoprotein E
LUM	ENSBTAG00000001745	ENSG00000139329	LUM	lumican
ITIH1	ENSBTAG00000007843	ENSG00000055957	ITIH1	inter-alpha-trypsin inhibitor heavy chain 1
C4BPA	ENSBTAG00000009876	ENSG00000123838	C4BPA	complement component 4 binding protein alpha
COTL1	ENSBTAG00000016315	ENSG00000103187	COTL1	coactosin like F-actin binding protein 1
KLKB1	ENSBTAG00000009501	ENSG00000164344	KLKB1	kallikrein B1
A1BG	ENSBTAG00000009735	ENSG00000121410	A1BG	alpha-1-B glycoprotein
APOD	ENSBTAG00000023600	ENSG00000189058	APOD	apolipoprotein D
APOA4	ENSBTAG00000019770	ENSG00000110244	APOA4	apolipoprotein A4
ITIH4	ENSBTAG00000007850	ENSG00000055955	ITIH4	inter-alpha-trypsin inhibitor heavy chain 4
VNN1	ENSBTAG00000015094	ENSG00000112299	VNN1	vanin 1
FETUB	ENSBTAG00000017531	ENSG00000090512	FETUB	fetuin B
LDHB	ENSBTAG00000019603	ENSG00000111716	LDHB	lactate dehydrogenase B
CHIA	ENSBTAG00000000259	ENSG00000134216	CHIA	chitinase acidic
PRDX2	ENSBTAG00000012062	ENSG00000167815	PRDX2	peroxiredoxin 2
RGN	ENSBTAG00000046155	ENSG00000130988	RGN	regucalcin

Table 9
Outlier ortholog genes across experimental conditions using FBS proteins.

Gene	Specie	TI-CT	Ti-CT-CH-TPP-PPHE
LDHB	hBM-MSCs	No	No
LDHB	FBS	No	No
PRDX2	hBM-MSCs	No	Yes
PRDX2	FBS	No	No
APOA1	hBM-MSCs	No	Yes
APOA1	FBS	Yes	Yes

viability of cells. As an example, Vester et al. [46] showed that green tea extracts protected human primary osteoblasts in the presence of oxidative stress induced by hydrogen peroxide, as was shown by the increased cell viability.

To further assess the safety of the proposed functionalization, an immunocompatibility study was performed using PBMCs to evaluate immune cell populations. Our results showed that the functionalized titanium discs (Ti-CT-CH-TPP-PPHE) did not induce disruptions to the immune cell subsets. However, biomaterials may create an unfavorable immune microenvironment that hinders bone regeneration and contributes to implant failure. Therefore, researchers have investigated various strategies, such as the modification of the surface characteristics of the implant and the utilization of local delivery systems with bioactive molecules, to create an optimal bone microenvironment for tissue regeneration [47]. Using titanium as a bulk material, Wang et al. [48] immobilized Zn^{2+} (an immunomodulatory metal ion), whereas Liu et al. [49] fabricated an interleukin-4/polydopamine (IL-4/PDA) coating. Both groups were able to achieve immunomodulation, favoring bone regeneration and successful implantation. In our study, the proposed functionalization did not interfere with the immune system function, which can be considered a positive result given the absence of simulated pro-inflammatory condition.

Moreover, our study compared the proteomic profile of hBM-MSCs on polyphenol-functionalized titanium (Ti-CT-CH-TPP-PPHE) against the control surface (Ti-CT) to elucidate the molecular mechanisms by which polyphenols enhance cellular functions critical for osteointegration. Both the GO terms detected using DAVID and those detected using the STRING database were evaluated. A key finding was the downregulation of proteins associated with “intermediate filament organization.” The cytoskeleton, composed of intermediate filaments, microfilaments, and microtubules, dictates cell shape, motility, and signal transduction [50]. The observed downregulation of intermediate filament components may suggest a dynamic and controlled restructuring of the cytoskeleton of hBM-MSCs in contact with the polyphenol-functionalized titanium. This process is a prerequisite for cells to adapt their shape for a robust cell-material interaction, migration, and mechanosensitivity, which in turn can impact osteogenic differentiation [51,52].

This active cellular adaptation is further supported by the complex changes observed in protein synthesis pathways. While the general term “translation” was downregulated, we observed a strong and specific upregulation of processes, such as “cytoplasmic translation” and “protein folding.” It is well-known that ECM organization plays crucial roles, such as in the development and tissue repair [53]. Thus, our finding may suggest that hBM-MSCs on polyphenol-functionalized titanium appear to be shifting their resources by downregulating the synthesis of general proteins while simultaneously upregulating the production of specific proteins required for cellular adhesion, signaling, as well as new ECM production and ECM remodeling. This targeted increase in protein synthesis is in accordance with the known effects of flavanols on cellular pathways related to bone homeostasis ([45]. Taken together, these proteomic changes may suggest that the interaction with polyphenols triggers a cascade of events in hBM-MSCS, which are cytoskeletal remodeling and targeted protein synthesis. To validate these findings and further strengthen our proposed mechanism, future work should include assays related to cytoskeletal reorganization, and the expression of key proteins involved in filament organization, protein synthesis and osteogenic differentiation pathway.

The GO terms detected using DAVID of the FBS proteins that exhibited positive adsorption to the Ti-CT-CH-TPP-PPHE disc surfaces in comparison to the control (Ti-CT) highlighted “Negative regulation of endopeptidase activity”. The regulation of endopeptidase activity is a complex process, and its regulation is essential for the maintenance of

protein homeostasis [54,55] and is crucial for various cellular processes [56]. Moreover, our analysis revealed that the PPHE-functionalized titanium surface (Ti-CT-CH-TPP-PPHE) interacts with several proteins involved in key immune processes. The presence of proteins associated with "immunoglobulin production involved in immunoglobulin-mediated immune response" and "antigen processing and presentation of peptide antigen via MHC class I", and "peptide antigen assembly with MHC class II protein complex" may suggest a potential engagement with pathways relevant to the adaptive immune system. Furthermore, the observed "positive regulation of immune response" may hint at a possible immunomodulatory effect. However, these findings are derived from studies with FBS proteins. While FBS served as a valuable initial platform for identifying protein interactions in our work, direct conclusions regarding human immunomodulation cannot be definitively drawn from these results alone. So, further studies are still necessary to validate these findings.

In our study, we were unable to demonstrate the antibacterial properties of CH or the polyphenolic extract. CH and its derivatives have broad-spectrum activity against Gram-positive and Gram-negative bacteria [57]. Still, these properties are susceptible to alterations due to factors such as pH, the type of microorganism, molecular weight concentration, and degree of deacetylation of CH [58,59]. In fact, the decreased antibacterial activity of CH added to titanium was also reported by other authors [60]. On the other hand, polyphenols have been found to possess antibacterial and antioxidant properties [61]. However, polyphenolic extracts have been primarily investigated for their antibacterial properties in the context of food preservation, and the findings have been inconsistent. Bouarab-Chibane et al. [62] reported that the effects can range from bacterial growth stimulation to antibacterial activity. The observed inconsistency in the antibacterial effects of polyphenolic extracts may explain the lack of potential of the polyphenolic extract investigated in this study to halt biofilm formation.

Finally, the outliers' analysis performed on the cellular proteomic data suggested that the chemically treated titanium (Ti-CT) surface results in changes in BM-MSCs by influencing processes related to membrane repair, extracellular matrix organization, cellular signaling involving phospholipids and calcium, and pathways related to prostaglandin metabolism. On the other hand, Ti-CT-CH-TPP-PPHE may influence BM-MSC behavior by affecting processes related to vesicle trafficking, wound healing, cell-cell adhesion mechanisms mediated by cadherins, and interactions with the extracellular environment, potentially involving exosomes and other extracellular vesicles. The predicted transcription factor regulation and the involvement of prostaglandin synthesis, further suggest complex cellular responses to this specific surface. However, these observations require further investigation to confirm their significance and elucidate the underlying mechanisms. Furthermore, the identification of PRDX2 and APOA1 as outlier orthologs in human BM-MSCs exposed to Ti-CT-CH-TPP-PPHE may suggest that this surface may trigger conserved responses across species related to redox balance via PRDX2 [63] and lipid metabolism via APOA1 [64] in these cells. Yet, further investigation with larger datasets and targeted assays would be necessary to validate these potential bioactivities.

This study has several limitations that should be acknowledged. The primary limitation is the lack of functional data confirming osteogenic differentiation. Future work must include quantitative assays, such as alkaline phosphatase (ALP) activity and matrix mineralization at relevant time points (e.g., 7 and 14 days). While the proteomics analysis provided preliminary data, it was insufficient to establish a clear mechanistic explanation for the observed cellular responses. Future research should aim to identify the specific signaling pathways being modulated by the coating. The conclusion of the absence of pro-inflammatory effects is preliminary. The assessment was based on the immunocompatibility study performed using PBMCs. Future work can include a quantitative analysis of key pro-inflammatory and anti-inflammatory cytokines to better characterize the material's immunomodulatory profile. The evaluation of antibacterial properties was restricted to a single bacterial species, *S. aureus*. However, the efficacy must be tested against a wider panel of relevant pathogens to ascertain the clinical applicability. From a materials science standpoint, the study did not quantify the polyphenol grafting density, as well as the coating's long-term stability and its release kinetics under simulated physiological conditions, which will be investigated in future works.

5. Conclusions

In summary, the PPHE extract obtained from unfermented seeds of the white grape *Moscato Bianco* resulted in a high polyphenolic content rich in flavanols without anthocyanins or flavonols. This composition, along with the formation of calcium–polyphenol complexes in the functionalization solution, led to improved solubility and antioxidant activity. Functionalization of the CH coating by PPHE was confirmed by fluorescence microscopy and XPS, which also revealed residual acetylation of CH.

Concerning the biological investigation, our study reveals novel interaction patterns between CH and polyphenols with hBM-MSCs and FBS proteins. While CH itself demonstrated minimal cytotoxicity, it did not promote cell adhesion and spreading. The addition of polyphenols, however, significantly enhanced cell metabolic activity and improved cell adhesion. Immunocompatibility studies further indicated that the functionalized specimens did not elicit an adverse immune response, thus being well-immune-tolerated. Cellular proteomic analysis suggests that the Ti-CT-CH-TPP-PPHE modification induces changes in cytoskeleton structure and protein synthesis, which may be linked to active remodeling. Finally, outlier analysis of cellular proteomic data suggests that the modified titanium surface influences several key cellular processes. Taken together, these findings underscore the context-dependent nature of biomaterial biocompatibility and suggest that the proposed functionalization strategy holds promise for enhancing cell-material interactions, though further investigation is needed to fully elucidate the underlying mechanisms and validate these findings for clinical applications.

CRediT authorship contribution statement

Farah Daou: Writing – original draft, Investigation. **Camilla Reggio:** Writing – original draft, Investigation. **Marcello Manfredi:** Writing – original draft, Methodology, Investigation. **Hugo Abreu:** Writing – original draft, Investigation. **Giuseppe Cappellano:** Writing – original draft, Methodology, Investigation. **Mauro Nascimben:** Writing – original draft, Methodology, Investigation. **Gissur Örlygsson:** Writing – original draft, Methodology, Investigation, Funding acquisition. **Chuen H. Ng:** Writing – original draft, Methodology, Investigation, Funding acquisition. **Antonella Bosso:** Writing – original draft, Investigation, Funding acquisition. **Sara Ferraris:** Writing – original draft, Methodology, Investigation, Conceptualization. **Silvia Spriano:** Writing – original draft, Supervision, Project administration, Methodology, Funding acquisition, Conceptualization. **Andrea Cochis:** Writing – original draft, Supervision, Methodology, Investigation, Conceptualization.

Declaration of competing interest

The Authors declare to have no conflicts of interest.

Acknowledgements

EU Commission, MUR, and the Icelandic Technology Development Fund are acknowledged for funding the NAT4MORE project (M.ERA-NET 2016).

Appendix A. Supplementary data

Supplementary data to this article can be found online at https://doi.org/10.1016/j.bioadv.2025.214584.

Data availability

No data was used for the research described in the article.

References

[1] A.A. Basson, J. Mann, M. Findler, G. Chodick, Correlates of early dental implant failure: a retrospective study, Int. J. Oral Maxillofac. Implants 38 (2023) 897–906, https://doi.org/10.11607/jomi.10199.

[2] J.T. Evans, J.P. Evans, R.W. Walker, A.W. Blom, M.R. Whitehouse, A. Sayers, How long does a hip replacement last? A systematic review and meta-analysis of case series and national registry reports with more than 15 years of follow-up, Lancet (London, England) 393 (10172) (2019) 647–654, https://doi.org/10.1016/S0140-6736(18)31665-9.

[3] N. Donos, A. Akcali, N. Padhye, A. Sculean, E. Calciolari, Bone regeneration in implant dentistry: which are the factors affecting the clinical outcome? Periodontol 2000 (93) (2023) 26–55, https://doi.org/10.1111/prd.12518.

[4] N. Walter, T. Stich, D. Docheva, V. Alt, M. Rupp, Evolution of implants and advancements for osseointegration: a narrative review, Injury 53 (Suppl. 3) (2022) S69–S73, https://doi.org/10.1016/j.injury.2022.05.057.

[5] O. Riester, M. Borgolte, R. Csuk, H.P. Deigner, Challenges in bone tissue regeneration: stem cell therapy, biofunctionality and antimicrobial properties of novel materials and its evolution, Int. J. Mol. Sci. 22 (2020) 192, https://doi.org/10.3390/ijms22010192.

[6] A. Josyula, K.S. Parikh, I. Pitha, L.M. Ensign, Engineering biomaterials to prevent post-operative infection and fibrosis, Drug Deliv. Transl. Res. 11 (2021) 1675–1688, https://doi.org/10.1007/s13346-021-00955-0.

[7] J. Quinn, R. McFadden, C.-W. Chan, L. Carson, Titanium for orthopedic applications: an overview of surface modification to improve biocompatibility and prevent bacterial biofilm formation, iSci 23 (11) (2020) 101745, https://doi.org/10.1016/j.isci.2020.101745.

[8] T. Stich, F. Alagboso, T. Křenek, T. Kovářík, V. Alt, D. Docheva, Implant-bone-interface: reviewing the impact of titanium surface modifications on osteogenic processes *in vitro* and *in vivo*, Bioeng. Transl. Med. 12 (7(1)) (2021) e10239, https://doi.org/10.1002/btm2.10239.

[9] S. Long, J. Zhu, Y. Jing, S. He, L. Cheng, Z. Shi, A comprehensive review of surface modification techniques for enhancing the biocompatibility of 3D-printed titanium implants, Coatings 13 (2023) 1917, https://doi.org/10.3390/coatings13111917.

[10] N. López-Valverde, J. Aragoneses, A. López-Valverde, C. Rodríguez, B. Macedo de Sousa, J.M. Aragoneses, Role of chitosan in titanium coatings. trends and new generations of coatings, Front. Bioeng. Biotech. 10 (2022) 907589, https://doi.org/10.3389/fbioe.2022.907589.

[11] M. Villegas, Y. Zhang, M. Badv, C. Alonso-Cantu, D. Wilson, Z. Hosseinidoust, T. F. Didar, Enhancing osseointegration and mitigating bacterial biofilms on medical-grade titanium with chitosan-conjugated liquid-infused coatings, Sci. Rep. 12 (2022) 5380, https://doi.org/10.1038/s41598-022-09378-4.

[12] D. Wu, J. Zhou, M.N. Creyer, W. Yim, Z. Chen, P.B. Messersmith, J.V. Jokerst, Phenolic-enabled nanotechnology: versatile particle engineering for biomedicine, Chem. Soc. Rev. 50 (2021) 4432–4483, https://doi.org/10.1039/d0cs00908c.

[13] G. Riccucci, M. Cazzola, S. Ferraris, V.A. Gobbo, M. Guaita, S. Spriano, Surface functionalization of Ti6Al4V with an extract of polyphenols from red grape pomace, Mater. Des. 206 (2021) 109776, https://doi.org/10.1016/j.matdes.2021.109776.

[14] A. Shavandi, A.E.A. Bekhit, P. Saeedi, Z. Izadifar, A.A. Bekhit, A. Khademhosseini, Polyphenol uses in biomaterials engineering, Biomater. 167 (2018) 91–106, https://doi.org/10.1016/j.biomaterials.2018.03.018.

[15] M. Mir, D.E. Wilson, A polyphenol decorated triplex hybrid biomaterial: structure–function, release profiles, sorption, and antipathogenic effects, ACS Appl. Bio Mater. 7 (11) (2024) 7391–7403.

[16] G. Riccucci, S. Ferraris, C. Reggio, A. Bosso, G. Örlygsson, C.H. Ng, S. Spriano, Polyphenols from grape pomace: functionalization of chitosan-coated hydroxyapatite for modulated swelling and release of polyphenols, Langmuir 37 (2021) 4793–14804, https://doi.org/10.1021/acs.langmuir.1c01930.

[17] W. Guo, X. Ding, H. Zhang, Z. Liu, Y. Han, Q. Wei, O.V. Okoro, A. Shavandi, L. Nie, Recent advances of chitosan-based hydrogels for skin-wound dressings, Gels 29 (10 (3)) (2024) 175, https://doi.org/10.3390/gels10030175.

[18] Y. Sun, T. Miao, Y. Wang, X. Wang, J. Lin, N. Zhao, Y. Hu, F.-J. Xu, A natural polyphenol-functionalized chitosan/gelatin sponge for accelerating hemostasis and infected wound healing, Biomater. Sci. 11 (2023) 2405–2418, https://doi.org/10.1039/D2BM02049A.

[19] S. Spriano, E. Verne', S. Ferraris, Patent number EP2214732B1, Multifunctional Titanium Surfaces for Bone Integration, 2008.

[20] M. Guaita, S. Motta, S. Messina, F. Casini, A. Bosso, Polyphenolic profile and antioxidant activity of green extracts from grape pomace skins and seeds of Italian cultivars, Foods 12 (2023) 3880, https://doi.org/10.3390/foods12203880.

[21] M.A. Bustamante, R. Moral, C. Paredes, A. Pérez-Espinosa, J. Moreno-Caselles, M. D. Pérez-Murcia, Agrochemical characterization of the solid by-products and residues from the winery and distillery industry, Waste Manag. 28 (2008) 372–380, https://doi.org/10.1016/j.wasman.2007.01.013.

[22] K. Dwyer, F. Hosseinian, M.R. Rod, The market potential of grape waste alternatives, J. Food Res. 3 (2014) 91, https://doi.org/10.5539/jfr.v3n2p91.

[23] M. Guaita, A. Bosso, Polyphenolic characterization of grape skins and seeds of four Italian red cultivars at harvest and after fermentative maceration, Foods 8 (2019) 395, https://doi.org/10.3390/foods8090395.

[24] G. Riccucci, M. Cazzola, S. Ferraris, V.A. Gobbo, M. Miola, A. Bosso, G. Örlygsson, C.H. Ng, E. Verné, S. Spriano, Surface functionalization of bioactive glasses and hydroxyapatite with polyphenols from organic red grape pomace, J. Am.Ceram. Soc. 105 (2022) 1697–1710, https://doi.org/10.1111/jace.17849.

[25] S. James, J. Fox, F. Afsari, J. Lee, S. Clough, C. Knight, J. Ashmore, P. Ashton, O. Preham, M. Hoogduijn, R. Ponzoni, Y. Hancock, M. Coles, P. Genever, Multiparameter analysis of human bone marrow stromal cells identifies distinct immunomodulatory and differentiation-competent subtypes, Stem Cell Rep. 4 (2015) 1004–1015, https://doi.org/10.1016/j.stemcr.2015.05.005.

[26] H. Abreu, M. Lallukka, D. Raineri, M. Leigheb, M. Ronga, G. Cappellano, S. Spriano, A. Chiocchetti, Evaluation of the immune response of peripheral blood mononuclear cells cultured on Ti6Al4V-ELI polished or etched surfaces, Front. Bioeng. Biotechnol. 12 (2024) 1458091, https://doi.org/10.3389/fbioe.2024.1458091.

[27] H. Abreu, M. Lallukka, M. Miola, S. Spriano, E. Vernè, D. Raineri, M. Leigheb, M. Ronga, G. Cappellano, A. Chiocchetti, Human T-cell responses to metallic ion-doped bioactive glasses, Int. J. Mol. Sci. 25 (8) (2024) 4501, https://doi.org/10.3390/ijms25084501.

[28] D. Szklarczyk, A. Franceschini, S. Wyder, K. Forslund, D. Heller, J. Huerta-Cepas, M. Simonovic, A. Roth, A. Santos, K.P. Tsafou, M. Kuhn, P. Bork, L.J. Jensen, C. von Mering, STRING v10: protein-protein interaction networks, integrated over the tree of life, Nucleic Acids Res. 43 (Database issue) (2015) D447–D452.

[29] L. McInnes, J. Healy, J. Melville, UMAP: uniform manifold approximation and projection for dimension reduction. In arXiv [stat.ML]. http://arxiv.org/abs/1802.03426, 2018.

[30] F.T. Liu, K.M. Ting, Z.-H. Zhou, Isolation forest, in: 2008 Eighth IEEE International Conference on Data Mining, 2008, pp. 413–422.

[31] Liis Kolberg, Uku Raudvere, Ivan Kuzmin, Priit Adler, Jaak Vilo, Hedi Peterson, g: Profiler—interoperable web service for functional enrichment analysis and gene identifier mapping (2023 update), Nucleic Acids Res. 51 (W1) (5 July 2023) W207–W212, https://doi.org/10.1093/nar/gkad347.

[32] L. Lu, Y. Li, X. Lu, Kinetic study of the complexation of gallic acid with Fe(II), Spectrochim. Acta, Part A 74 (2009) 829–834, https://doi.org/10.1016/j.saa.2009.08.025.

[33] N.R. Perron, J.L. Brumaghim, A review of the antioxidant mechanism of polyphenols compounds related to iron binding, Cell Biochem. Biophys. 53 (2009) 75–100, https://doi.org/10.1007/s12013-009-9043-x.

[34] S. Ferraris, A. Cochis, M. Cazzola, M. Tortello, C.A. Scalia, S. Spriano, L. Rimondini, Cytocompatible and anti-bacterial adhesion nanotextured titanium oxide layer on titanium surfaces for dental and orthopedic implants, Front. Bioeng. Biotechnol. 7 (2019) 103, https://doi.org/10.3389/fbioe.2019.00103.

[35] S. Ferraris, G. Örlygsson, C.H. Ng, G. Riccucci, S. Spriano, Chemical, physical, and mechanical characterization of chitosan coatings on a chemically pre-treated Ti6Al4V alloy, Surf. Coat. Tech. 441 (2022) 128571, https://doi.org/10.1016/j.surfcoat.2022.128571.

[36] P.-C. Li, G.M. Liao, S.R. Kumar, C.-M. Shih, C.-C. Yang, D.-M. Wang, S.J. Lue, Fabrication and characterization of chitosan nanoparticle-incorporated quaternized poly(vinyl alcohol) composite membranes as solid electrolytes for direct methanol alkaline fuel cells, Electrochim. Acta 187 (2016) 616–628, https://doi.org/10.1016/j.electacta.2015.11.117.

[37] Y.P. Neo, S. Swift, S. Ray, M. Gizdavic-Nikolaidis, J. Jin, C.O. Perera, Evaluation of gallic acid loaded zein sub-micron electrospun fibre mats as novel active packaging materials, Food Chem. 141 (2013) 3192–3200, https://doi.org/10.1016/j.foodchem.2013.06.018.

[38] F. Gamna, S. Yamaguchi, A. Cochis, S. Ferraris, A. Kumar, L. Rimondini, S. Spriano, Conferring antioxidant activity to an antibacterial and bioactive titanium surface through the grafting of a natural extract, Nanomaterials 13 (2023) 479, https://doi.org/10.3390/nano13030479.

[39] Y. Kim, Z. Zharkinbekov, K. Raziyeva, L. Tabyldiyeva, K. Berikova, D. Zhumagul, K. Temirkhanova, A. Saparov, Chitosan-based biomaterials for tissue regeneration, Pharmaceutics 15 (2023) 807, https://doi.org/10.3390/pharmaceutics15030807.

[40] C. Reggio, J. Barberi, S. Ferraris, S. Spriano, Functionalization of Ti6Al4V alloy with polyphenols: the role of the titanium surface features and the addition of calcium ions on the adsorption mechanism, Metals 13 (2023) 1347, https://doi.org/10.3390/met13081347.

[41] K.E. Heim, A.R. Tagliaferro, D.J. Bobilya, Flavonoid antioxidants: chemistry, metabolism and structure-activity relationships, J. Nutr. Biochem. 13 (2002) 572–584, https://doi.org/10.1016/S0955-2863(02)00208-5.

[42] F. Shahidi, J. Yeo, Bioactivities of phenolics by focusing on suppression of chronic diseases: a review, Int. J. Mol. Sci. 19 (2018) 1573, https://doi.org/10.3390/ijms19061573.

[43] D. Bellavia, E. Dimarco, V. Costa, V. Carina, A. De Luca, L. Raimondi, M. Fini, C. Gentile, F. Caradonna, G. Giavaresi, Flavonoids in bone erosive diseases: perspectives in osteoporosis treatment, Trends Endocrinol. Metab. 32 (2021) 76–94, https://doi.org/10.1016/j.tem.2020.11.007.

[44] V. Rodríguez, M. Rivoira, G. Picotto, G.D. de Barboza, A. Collin, N. Tolosa de Talamoni, Analysis of the molecular mechanisms by flavonoids with potential use for osteoporosis prevention or therapy, Curr. Med. Chem. 29 (16) (2022) 2913–2936, https://doi.org/10.2174/0929867328666210921143644.

[45] A.R. Sharma, Y.H. Lee, A. Bat-Ulzii, S. Chatterjee, M. Bhattacharya, C. Chakraborty, S.S. Lee, Bioactivity, molecular mechanism, and targeted delivery of flavonoids for bone loss, Nutrients 15 (2023) 919, https://doi.org/10.3390/nu15040919 (PMID: 36839278; PMCID: PMC9960663).
[46] H. Vester, N. Holzer, M. Neumaier, S. Lilianna, A.K. Nüssler, C. Seeliger, Green tea extract (GTE) improves differentiation in human osteoblasts during oxidative stress, J. Inflamm. 11 (2014) 15, https://doi.org/10.1186/1476-9255-11-15.
[47] B. Lv, J. Wu, Y. Xiong, X. Xie, Z. Lin, B. Mi, G. Liu, Functionalized multidimensional biomaterials for bone microenvironment engineering applications: focus on osteoimmunomodulation, Front. Bioeng. Biotechnol. 10 (2022) 1023231, https://doi.org/10.3389/fbioe.2022.1023231.
[48] T. Wang, J. Bai, M. Lu, C. Huang, D. Geng, G. Chen, L. Wang, J. Qi, W. Cui, L. Deng, Engineering immunomodulatory and osteoinductive implant surfaces via mussel adhesion-mediated ion coordination and molecular clicking, Nat. Commun. 13 (2022) 160, https://doi.org/10.1038/s41467-021-27816-1.
[49] R. Liu, S. Chen, P. Huang, G. Liu, P. Luo, Z. Li, Y. Xiao, Z. Chen, Z. Chen, Immunomodulation-based strategy for improving soft tissue and metal implant integration and its implications in the development of metal soft tissue materials, Adv. Funct. Mater. 30 (2020) 190672, https://doi.org/10.1002/adfm.201910672.
[50] L. Chang, R. Goldman, Intermediate filaments mediate cytoskeletal crosstalk, Nat. Rev. Mol. Cell Biol. 5 (2004) 601–613, https://doi.org/10.1038/nrm1438.
[51] E. Infante, S. Etienne-Manneville, Intermediate filaments: Integration of cell mechanical properties during migration, Front. Cell Dev. Biol. 10 (2022) 951816, https://doi.org/10.3389/fcell.2022.951816.
[52] P.S. Mathieu, E.G. Loboa, Cytoskeletal and focal adhesion influences on mesenchymal stem cell shape, mechanical properties, and differentiation down osteogenic, adipogenic, and chondrogenic pathways, Tissue Eng. Part B Rev. 18 (6) (2012) 436–444, https://doi.org/10.1089/ten.TEB.2012.0014.
[53] M. Larsen, V.V. Artym, J.A. Green, K.M. Yamada, The matrix reorganized: extracellular matrix remodeling and integrin signaling, Curr. Opin. Cell Biol. 18 (2006) 463–471, https://doi.org/10.1016/j.ceb.2006.08.009.
[54] E.J. Cotter, N. von Offenberg Sweeney, P.M. Coen, Y.A. Birney, M.J. Glucksman, P. A. Cahill, P.M. Cummins, Regulation of endopeptidases EC3.4.24.15 and EC3.4.24.16 in vascular endothelial cells by cyclic strain: role of Gi protein signaling, Arterioscler. Thromb. Vasc. Biol. 24 (3) (2004) 457–463, https://doi.org/10.1161/01.ATV.0000117176.71143.a1.
[55] S.I. Kim, A. Pabon, T.A. Swanson, M.J. Glucksman, Regulation of cell-surface major histocompatibility complex class I expression by the endopeptidase EC3.4.24.15 (thimet oligopeptidase), Biochem. J. 375 (Pt 1) (2003) 111–120, https://doi.org/10.1042/BJ20030490.
[56] C. López-Otín, J.S. Bond, Proteases: multifunctional enzymes in life and disease, J. Biol. Chem. 283 (45) (2008) 30433–30437, https://doi.org/10.1074/jbc.R800035200.
[57] M. Másson, Antimicrobial properties of chitosan and its derivatives, in: R. Jayakumar, M. Prabaharan (Eds.), Chitosan for Biomaterials III. Advances in Polymer Science vol 287, Springer, Cham, 2021, https://doi.org/10.1007/12_2021_104.
[58] J. Fourie, F. Taute, L. du Preez, D. de Beer, Chitosan composite biomaterials for bone tissue engineering—a review, Regen. Eng. Transl. Med. 8 (2022) 1–21, https://doi.org/10.1007/s40883-020-00187-7.
[59] C.-L. Ke, F.-S. Deng, C.-Y. Chuang, C.-H. Lin, Antimicrobial actions and applications of chitosan, Polym 13 (2021) 904, https://doi.org/10.3390/polym13060904.
[60] K. Kavitha, S. Sutha, M. Prabhu, V. Rajendran, T. Jayakumar, In situ synthesized novel biocompatible titania-chitosan nanocomposites with high surface area and antibacterial activity, Carbohydr. Polym. 93 (2013) 731–739, https://doi.org/10.1016/j.carbpol.2012.12.031.
[61] X. Gao, Z. Xu, G. Liu, J. Wu, Polyphenols as a versatile component in tissue engineering, Acta Biomater. 119 (2021) 57–74, https://doi.org/10.1016/j.actbio.2020.11.004.
[62] L. Bouarab-Chibane, V. Forquet, P. Lantéri, Y. Clément, L. Léonard-Akkari, N. Oulahal, P. Degraeve, C. Bordes, Antibacterial properties of polyphenols: characterization and QSAR (quantitative structure-activity relationship) models, Front. Microbiol. 10 (2019) 829, https://doi.org/10.3389/fmicb.2019.00829.
[63] P. Balasubramanian, V. Vijayarangam, M.K.G. Deviparasakthi, T. Palaniyandi, M. Ravi, S. Natarajan, S. Viswanathan, G. Baskar, M.R.A. Wahab, H. Surendran, Implications and progression of peroxiredoxin 2 (PRDX2) in various human diseases, Pathol. Res. Pract. 254 (2024) 155080, https://doi.org/10.1016/j.prp.2023.155080.
[64] X. Su, D. Peng, The exchangeable apolipoproteins in lipid metabolism and obesity, Clin. Chim. Acta 503 (2020) 128–135, https://doi.org/10.1016/j.cca.2020.01.015.
[65] G. Zhu, G. Wang, J.J. Li, Advances in implant surface modifications to improve osseointegration, Mater. Adv. 2 (2021) 6901–6927, https://doi.org/10.1039/D1MA00675D.
[66] INTERNATIONAL STANDARD ISO 10993-5, Biological evaluation of medical devices — Part 5: Tests for in vitro cytotoxicity, Third edition, 2009-06-01.
[67] Z. Pang, Y. Lu, G. Zhou, F. Hui, L. Xu, C. Viau, A.F. Spigelman, P.E. MacDonald, D. S. Wishart, S. Li, J. Xia, MetaboAnalyst 6.0: towards a unified platform for metabolomics data processing, analysis and interpretation, Nucleic Acids Res. 52 (W1) (2024 Jul 5) W398–W406, https://doi.org/10.1093/nar/gkae253. PMID: 38587201; PMCID: PMC11223798.